

Jumping VaR: Order Statistics Volatility Estimator for Jumps Classification and Market Risk Modeling*

Luca Spadafora^{†1,2}, Francesca Sivero¹ and Nicola Picchiotti¹

¹Internal Model Validation, Banco BPM S.p.A., Piazza F. Meda 4, 20121 Milano, Italy

²Department of Computer Sciences, University of Verona, Verona, Italy

Abstract

This paper proposes a new integrated variance estimator based on order statistics within the framework of jump-diffusion models. Its ability to disentangle the integrated variance from the total process quadratic variation is confirmed by both simulated and empirical tests. For practical purposes, we introduce an iterative algorithm¹ to estimate the time-varying volatility and the occurred jumps of log-return time series. Such estimates enable the definition of a new market risk model for the Value at Risk forecasting. We show empirically that this procedure outperforms the standard historical simulation method applying standard back-testing approach.

Keywords: Integrated variance, Jump estimates, Jumping VaR model, Order statistic estimator, Time-varying volatility, Threshold estimator, VaR, Back-testing, FRTB.

1 Introduction

The Basel Committee requires that a certain amount of capital is held by financial firms as protection from market risk. According to the recent Fundamental Review of Trading Book (FRTB) Banking Supervision (2012, 2013, 2014), in case of internal model approach, the risk measure involved in the computation of the capital requirement moves from Value at Risk (VaR) to Expected Shortfall (ES). Nevertheless, the Value at Risk remains the measure required for back-testing purposes. In particular, FRTB strengthened the VaR back-testing requirements at portfolio level, where jumping behaviour of time series is not off-setted or smoothed by the aggregation of many instruments. In addition, even if VaR computation is typically required for time horizons that range from 10 days to one year, in practical applications VaR is usually estimated over a shorter time horizon, e.g. one day, in order to exploit a larger dataset, and then it is projected up to required time horizon, with suitable scaling formulas (see Spadafora (2014) and the references therein). As a consequence, back-testing analyses are typically performed on short time horizons, where the jumping behaviour can be relevant. For this reason, the definition of a market risk model allowing to produce accurate VaR predictions endures as research topic and we chose it as field to which provide our contribution.

Noting that the presence of large fluctuations in asset log-returns is responsible for part of the poor back-testing performances of the standard historical simulation VaR method, we propose a new approach that distinguishes the past realizations into ordinary and jump ones and includes this information in the VaR prediction. More precisely, in order to achieve this goal, as a first step, we defined a new integrated variance estimator based on order statistics, proposing an iterative algorithm to estimate the time-varying volatility and the occurred jumps of log-return times series, and, secondly, we introduced a new method for VaR forecasting that models the jumping behaviour of the time series with an ad-hoc

*The views, thoughts and opinions expressed in this paper are those of the authors in their individual capacity and should not be attributed to Banco BPM S.p.A. or to the authors as representatives or employees of Banco BPM S.p.A. The authors are grateful to the Elisabetta Benzi, Cecilia Mancini, Roberto Renò for helpful comments and suggestions on the topic.

[†]Corresponding Author, luca.spadafora@gmail.com

¹available on the website <https://github.com/sigmaquadro/VolatilityEstimator>

approach, specific for the jumping component.

The outline of the paper is the following. In Section 2 we revise the existing literature related to the topics discussed in the paper. Section 3 presents the mathematical framework and the definition of the order statistic volatility estimator, introducing algorithms for its implementation, while Section 4 shows its ability to disentangle the integrated variance from the total process quadratic variation by simulated and empirical tests. Section 5 describes a sanity check that we performed on empirical data to verify whether the initial assumptions of our model held true. In Section 6 we introduce a new market risk model for VaR estimation based on the outcomes of the order statistic volatility estimator. Finally, in Section 7, we empirically back-test the Jumping VaR model comparing its performances with the ones of other standard and advanced VaR forecasting models. In Section 8 we provide our conclusions.

2 Literature Review

The presence of jumps (large fluctuations) in asset return time series has been confirmed by a wide variety of empirical studies. In many recent works such asset returns are modeled by jump-diffusion dynamics and the issue of disentangling the continuous part of the stochastic process from the jump one has been faced. For instance, Ait-Sahalia (2004) has proven the asymptotic ability of the MLE to estimate the volatility of log-returns cleaned up from the noise due to the jump component, considering Poisson jump diffusion processes (finite jump activity) and extending the results to Cauchy jump diffusion processes (specific cases of infinite jump activity). Shephard et al. (2003) have proposed a model-free estimator of the continuous and the jump part of the quadratic variation for stochastic volatility models in case of finite activity jumps, based on the realized power and bipower variations. This study on the realized multipower variation estimator has also been extended to the case of infinite activity jump processes in Barndorff-Nielsen et al. (2006) proving the robustness of such estimator also in case of infinite activity Lévy processes, with activity not too high, and providing asymptotic distributions of the realized multipower variation when there are jumps. Mancini (2009) has presented a non-parametric threshold estimator of the integrated variance for a jump-diffusion model with finite or infinite jump activity, providing also asymptotic results and giving, in case of finite jump activity, a non-parametric estimate of the jump times. We mainly consider this paper and Mancini et al. (2011) as a starting point for our contribution. Additional details on this estimator can be found in Spadafora et al. (2017).

While several authors have focused their research on jump-diffusion models to describe the asset return dynamics, it is worth noting that Carr et al. (2002) and Geman (2002) have pointed out that pure jump Lévy processes can be used to model asset returns in a more realistic way, substituting the continuous part with infinite small jumps due to the infinite activity jump component of the Lévy process.

The issue of including asset return jumps in the Value at Risk forecasting has been approached in several papers in the last years. A wide range of these works aims at computing the VaR via parametric methods, supposing jump-diffusion dynamics of the asset log-returns. For instance, Pan et al. (2001) have suggested computing VaR by applying the Inverse Fourier Transform to the characteristic function of the portfolio log-return process approximated via delta-gamma approach, while Szerszen (2009) has implemented the VaR forecasting based on jump-diffusion models, including stochastic volatility and both finite and infinite activity jump components, and on the model specification estimation via Bayesian MCMC (Markov Chain Monte Carlo). Moreover, further related works include Guan et al. (2004) and Chen (2010) proposing analytical VaR computation in jump diffusion model framework. Less research has been performed on the VaR prediction including jumps through the non-parametric method of the historical simulation. In this regard, Gibson (2001) has proposed an algorithm to compute VaR based on both the variance-covariance and on the historical simulation method, modeling the loss process as sum of an ordinary component and a jump one described by a trinomial distribution and also pointing out the need to add the correlation among jump times to better capture the real asset return dynamics.

3 Volatility Estimator

3.1 Introduction

Starting from the non-parametric threshold estimator introduced in Mancini (2009), we propose an estimator of the integrated variance of jump-diffusion stochastic processes, based on order statistics. As a result, estimates of the process time-varying volatility can be obtained by an iterative method and they can be employed for practical purposes, for example for market risk modeling.

In this section we provide a simple introduction to the estimator, describing the intuition behind it. As a consequence, we intentionally avoided some accuracy in the approach in favour to a better description of the general idea. In the following sections, we provide a formal mathematical description of the statistical estimator we want to introduce.

In a nutshell, we want to obtain a definition of a jump as a realization that is abnormal and anomalous with respect to the other realizations in our time series. For this reason, we need to consider a reference distribution (in the rest of the paper we consider a Gaussian distribution even if the approach can be easily extended to other distributions) and we need to evaluate if a given realization is compatible with it. A typical approach in this case could be to classify as jump (as anomalous realization) all realizations that lie far from the centre of the distribution. A very naive approach could be for example to consider some multiple of the standard deviation of the time series and assume that all the realizations larger (or smaller) than this (negative) threshold are outliers. In our view, this approach is rather rough, as *all* the realizations above (or below) the (negative) threshold are classified as jumps. On the contrary, it could happen that many realizations do not lie too far from the centre of the distribution, but they are simply too frequent for the reference distribution. A very simple example could be obtained if one considers a T-Student distribution for the realizations and a Gaussian distribution as a reference. As the T-Student distribution has fat tails, once a sufficiently large (in absolute terms) threshold is defined, many realizations will lie below the threshold, even if their frequency is not compatible with a Gaussian distribution. In other words, for a given threshold, only the really extreme realization will be classified as jump, but the tail of the distribution will remain fatter than the one implied by a Gaussian distribution. In any cases, it can be proved that there exists a smart way to define this threshold in order to obtain estimators that satisfy typical statistical convergence requirements Mancini (2009). In this paper we want to develop a different approach that is able to go beyond the truncation effect given by the definition of the threshold while maintaining most of the theoretical framework introduced in Mancini (2009) that represents our main reference. Essentially, the main idea of this paper is based on two key points:

- the mapping of the threshold definition problem into a probability threshold problem
- the introduction of extreme value theory as a statistical tool to identify jumps.

Concerning the first point, we transform the threshold problem in a statistical problem where we want to estimate what is the *probability* of observing a realization so large (or so small). Even if the two problems are equivalent as we just applied a mapping, we think that this step is relevant from a practical point of view because the definition of a probability threshold is typically easier to understand and to interpret than a threshold on a random variable.

With respect to the second point, we transform the statistical question from *what is the probability of observing a realization given a reference distribution?* to the question *what is the probability of getting a k -th maximum as the one observed if we could sample many times a time series of n realizations?* By this change in the approach, we are questioning if each ordered realization can be larger (or smaller) than the one observed; in this way, it could happen that the maximum is not large enough to be classified as jump, differently to the k -th maximum. In this way, in the above T-Student example, the frequency of largest (smallest) observations can be reduced, avoiding the problem of introducing a truncation of the distribution.

In the following sections, we provide a formal description of these simple ideas with both numerical and empirical examples.

3.2 Framework

According to the Lévy-Itô Decomposition, a Lévy process is characterized by the superposition of a continuous part, formed by a drift term and a Brownian motion, and independent Poisson processes,

possibly infinitely many, as reported in Tankov et al. (2015). Therefore, modeling the stock log-returns as realizations of a Lévy process, we consider the following set-up.

Let $\{Y_t\}_{t \in \mathbb{R}^+}$ be a stochastic process with dynamics

$$\begin{cases} dY_t = \sigma_t dW_t + dJ_t = dY_t^c + dJ_t & t > 0 \\ Y_0 = y_0 \in \mathbb{R} \end{cases} \quad (1)$$

where W_t is a standard Brownian motion, σ_t is the volatility of the continuous part of Y_t (named Y_t^c) and J_t is a pure jump process.

The pure jump process can have either finite activity (FA), i.e. finitely many “big” jumps can occur in finite time, or infinite activity (IA), i.e. an infinite number of “compensated small” jumps can occur in finite time interval.

Note that we assume the drift term to be negligible and thus we do not include it in the Y_t dynamics in Eq. 1.

The quadratic variation of the process Y_t corresponds to the sum of the quadratic variation of the continuous part, called integrated variance (IV), and the quadratic variation of the jump component (Tankov et al. (2015)). Formally,

$$[Y, Y]_t = [Y^c, Y^c]_t + \sum_{\substack{s \leq t \\ \Delta J_s \neq 0}} |\Delta J_s|^2 = \int_0^t \sigma_s^2 ds + \sum_{\substack{s \leq t \\ \Delta J_s \neq 0}} |\Delta J_s|^2 \quad (2)$$

Assuming that the realizations of the Y_t process are recorded at n discrete equispaced times $\delta t, \dots, n\delta t = T$, our aim is to estimate the integrated variance of the process disentangling it from the quadratic variation of the jump part.

Naming $Y_{\delta t}, Y_{2\delta t}, \dots, Y_{(n+1)\delta t}$ the $n + 1$ random variables obtained sampling Y_t in time, denote by $\Delta_i Y := Y_{(i+1)\delta t} - Y_{i\delta t}$ for $i = 1, \dots, n$ the discrete increments of Y_t and, likewise, $\Delta_i Y^c := Y_{(i+1)\delta t}^c - Y_{i\delta t}^c$ as the discrete increments of the continuous part of Y_t . The corresponding realizations of such random variables are indicated by lower-case letters, that is $\{\Delta_1 y, \dots, \Delta_n y\}$, on one hand, and $\{\Delta_1 y^c, \dots, \Delta_n y^c\}$, on the other hand. This notation will be kept throughout the whole paper.

3.3 Threshold Estimator

The non-parametric threshold estimator proposed in Mancini (2009) is defined as

$$\hat{IV}_{Thr} = \sum_{i=1}^n (\Delta_i Y)^2 \mathbb{1}_{\{|\Delta_i Y| \leq \sqrt{\theta(\delta t)}\}} \quad (3)$$

where $\theta(\delta t)$ is a threshold function that must satisfy $\lim_{\delta t \rightarrow 0} \theta(\delta t) = 0$ and $\lim_{\delta t \rightarrow 0} \frac{\delta t \log \frac{1}{\delta t}}{\theta(\delta t)} = 0$.

The Levy’s Modulus of Continuity Theorem (Sato (1999)) is the key result exploited to prove the consistency of this estimator. It states that

$$\lim_{\epsilon \rightarrow 0} \sup_{\substack{0 < t < 1 \\ 0 < s < \epsilon}} \frac{|W_{t+s} - W_t|}{\sqrt{2s \log \frac{1}{s}}} = 1 \quad (4)$$

almost surely. Therefore, considering the time grid $0, \delta t, \dots, n\delta t = T$, as enunciated in Mancini (2010) and Mancini (2009),

$$\mathbb{P} \left(\lim_{\delta t \rightarrow 0} \sup_{i=1, \dots, n} \frac{|W_{(i+1)\delta t} - W_{i\delta t}|}{\sqrt{2\delta t \log \frac{1}{\delta t}}} \leq 1 \right) = 1 \quad (5)$$

and, thus, keeping in mind the stochastic integral definition, the absolute value of any path of a stochastic integral with respect to a Brownian motion tends to zero almost surely as the function $\sqrt{2\delta t \log \frac{1}{\delta t}}$. As a

result, if $(\Delta_i Y)^2 > \theta(\delta t) > 2\delta t \log \frac{1}{\delta t}$ then, in the time interval δt , some jumps in the Y_t process must be occurred, when δt approaches zeros.

According to Mancini (2009), under the assumptions on the drift, the diffusion and the threshold function stated in the mentioned paper, the threshold estimator is *consistent* for both cases of finite and infinite activity jump part. Moreover, considering a process with only finite activity jump component and under the same set of hypotheses required for the consistency, the threshold estimator has a Normal asymptotic distribution (i.e. as $\delta t \rightarrow 0$, having fixed the grid time horizon T) with mean corresponding to the integrated variance and variance proportional to the inverse of the number of time steps at which the realizations of the stochastic process are recorded, fixed the time horizon of the grid. Consequently, the speed of convergence of the estimator to the true parameter depends on the square root of the number of time steps.

The hypotheses on the threshold function are necessary for the consistency of the estimator, although, in practice, we can observe the realizations of Y_t only at discrete times and thus the time step δt is fixed. Within this setting, the choice of the threshold function is not so easy. For example, the threshold function of the form $\theta(\delta t) := (\delta t)^\beta$ with $\beta \in]0, 1[$ suggested in Mancini (2009) is dominated by the $2\delta t \log \frac{1}{\delta t}$ only in the limit for $\delta t \rightarrow 0$ and thus, if δt is sufficiently high, the relation $(\Delta_i Y)^2 > \theta(\delta t) > 2\delta t \log \frac{1}{\delta t}$ does not hold anymore and some jumps could not be detected by the estimator. In addition, as $\Delta_i Y$ depends on the scale parameter σ , in order to assure that the relation holds, a suitable renormalization procedure must be considered in order to neutralize the effect of the scale parameter.

In accordance with this reasoning, in our implementation of the estimator in Eq. 3, we choose the threshold function exactly equal to

$$\bar{\theta}(\delta t) := 2 \log \frac{1}{\delta t} \quad (6)$$

rescaled by the sample variance of $\{\Delta_1 Y, \dots, \Delta_n Y\}$ (that is proportional to δt), obtaining a threshold proportional to $\delta t \log \frac{1}{\delta t}$.

It is worth noting that the choice of this threshold function agrees with the results proved in Figueroa-López et al. (2017) concerning the optimal threshold definition by means of the mean square error technique.

3.4 From Maximum to Order Statistics

Since Eq. 5 holds in the limit, in case of fixed δt the following relation must be true

$$\mathbb{P} \left(\max_{i=1, \dots, n} \frac{|W_{(i+1)\delta t} - W_{i\delta t}|}{\sqrt{2\delta t \log \frac{1}{\delta t}}} > 1 \right) = \bar{p} \iff \mathbb{P} \left(\max_{i=1, \dots, n} |W_{(i+1)\delta t} - W_{i\delta t}| > \sqrt{2\delta t \log \frac{1}{\delta t}} \right) = \bar{p} \quad (7)$$

where $\bar{p} \in [0, 1]$ is a certain probability value which refers to the random variable $\max_{i=1, \dots, n} |W_{(i+1)\delta t} - W_{i\delta t}|$.

Eq. 7 provides a link between the threshold exploited in Mancini (2009) in order to define the estimator reported in Eq. 3 and a probability threshold \bar{p} . In particular, by this formulation, the choice of the threshold $\bar{\theta}(\delta t)$ results into the definition of the confidence level (\bar{p}) corresponding to the error in the jump detection that one is willing to accept.

More in general, it is possible to extend this approach for a generic tolerance level p (without considering the absolute value)

$$\mathbb{P} \left(\max_{i=1, \dots, n} (W_{(i+1)\delta t} - W_{i\delta t}) > \theta^W \right) = p \quad (8)$$

for a threshold θ^W . Since in our approach, we want to invert Eq. 8 in order to obtain a threshold for a fixed value of the probability p , we make explicit this dependence using the notation $\theta^W(p; n, n)$, where the double n refers to the fact that the maximum operator in Eq. 8 can be interpreted as the n -th minimum of a sample made by n realizations. This notation will be exploited in the next sections, where we will generalize this setup. In addition, we apply our choice to consider a Gaussian cumulative

distribution function (c.d.f.) as a reference distribution, obtaining the following results

$$\begin{aligned}\theta^W(p; n, n) &= \sqrt{\delta t} \theta(p; n, n) \\ \theta(p; n, n) &= F_{Z_{n:n}}^{-1}(1-p)\end{aligned}\tag{9}$$

where $F_{Z_{n:n}}(x) = (\Phi(x))^n$ is the c.d.f. of the maximum of n Standard Normal random variables and $\Phi(x)$ is the c.d.f. of a Standard Normal random variable (refer to Appendix A.1 for further details on such derivation). As mentioned in Section 3.1, here we assume that our reference distribution is Normal but the approach can be easily extended to other reference distributions. The notation $Z_{k:j}$ stands for the k -th realization over an (increasing) ordered sample of j elements.

It is worth noting that, since the Normal distribution is symmetric, the random variables $Z_{n:n}$ and $-Z_{1:n}$ (where $Z_{1:n}$ is the minimum of n Standard Normal random variables) have the same distribution. In the following, we will consider Eq. 8 as starting point for the definition of our new volatility estimator.

In the light of the approximation stated in Appendix A.2, $\theta(p; n, n)$ multiplied by the square root of the sample variance of $\{\Delta_1 Y, \dots, \Delta_n Y\}$ can be set as threshold function to plug-in in Eq. 3 to estimate the IV of the Lévy process Y_t , once the tolerance level p is fixed (note that here we are assuming that the volatility is constant in time, whereas in the next section we will relax this hypothesis).

This choice implies that all the realizations in the set $\{\Delta_1 y, \dots, \Delta_n y\}$ larger, in absolute terms, than the maximum value acceptable for the discrete increments of Y_t^c are excluded from the IV computation.

Nevertheless, this choice does not take into account the possibility of having realizations in the set $\{\Delta_1 y, \dots, \Delta_n y\}$ which, even being smaller than the maximum acceptable value, are too frequent to be Gaussian and, thus, to be realizations of the discrete increments of Y_t^c only. According to this reasoning, the threshold $\theta(p; n, n)$ can be replaced by a realization-varying threshold $\theta(p; k, n')$, whose value depends on the progressive classification of the ordered realizations of $\{\Delta_1 y, \dots, \Delta_n y\}$.

More precisely, starting from Eq. 8 and substituting the maximum over the n observations with the k -th order statistic in the dataset of size n' , a more general threshold function $\theta(p; k, n')$ can be defined. Formally,

$$\begin{aligned}\mathbb{P}(k\text{-th ordered statistic in the dataset } \{(W_{(i+1)\delta t} - W_{i\delta t})\}_{i=1}^{n'} > \theta^W(p; k, n')) &= p \\ \Downarrow \\ \theta^W(p; k, n') = \sqrt{\delta t} \theta(p; k, n') \quad \text{and} \quad \theta(p; k, n') &= F_{Z_{k:n'}}^{-1}(1-p)\end{aligned}\tag{10}$$

where

$$F_{Z_{k:n'}}(x) = I_{\Phi(x)}(k, n' - k + 1) = \frac{n'!}{(k-1)!(n'-k)!} \int_0^{\Phi(x)} u^{k-1} (1-u)^{n'-k} du\tag{11}$$

is the c.d.f. of the k -th order statistic in the dataset of n' Standard Normal random variables and $I_x(a, b)$ is an Incomplete Beta function with parameters a, b . (The whole derivation of the threshold $\theta(p; k, n')$ is reported in Appendix A.1). Moreover, thanks to the symmetry of the Normal distribution, $Z_{k:n'}$ has the same distribution of $-Z_{(n'-k+1):n'}$.

Therefore, the procedure can be summarized as follows: $\{\Delta_1 y, \dots, \Delta_n y\}$ are ordered and the largest observation in this set is compared with the threshold $\theta(p; n, n)$ rescaled by the square root of the sample variance of $\{\Delta_1 y, \dots, \Delta_n y\}$; depending on whether the largest observation has been classified as jump or not, the threshold itself can be updated to $\theta(p; n-1, n-1)$ or $\theta(p; n-1, n)$, always rescaling by the square root of the sample variance of $\{\Delta_1 y, \dots, \Delta_n y\}$. The new threshold so obtained can then be compared with the second largest element in the sample and so on and so forth. The formal definition of such new estimator of the IV based on the order statistics theory is reported hereafter.

3.5 Order Statistic Estimator

First of all, we denote the ordered set of the discrete increments of the Y_t process as $\{\Delta_{n:n} Y, \dots, \Delta_{1:n} Y\}$ with $\Delta_{i:n-1} Y \leq \Delta_{(i+1):n} Y$ $i = 1, \dots, n$. Moreover, we introduce the increasing sequences of sets

$\{\mathcal{G}_i\}_{i=0}^m$ and $\{\mathcal{G}'_i\}_{i=0}^{m'}$, with $m = \lceil \frac{n}{2} \rceil$ and $m' = \lfloor \frac{n}{2} \rfloor$. Assuming n even for simplicity, we define

$$\begin{aligned} \mathcal{G}_0 &= \emptyset & \mathcal{G}_i &= \{I_1, \dots, I_i\} & i &= 1, \dots, m \\ \mathcal{G}'_0 &= \emptyset & \mathcal{G}'_i &= \{I'_1, \dots, I'_i\} & i &= 1, \dots, m' \end{aligned} \quad (12)$$

where I_i and I'_i are random variables progressively defined as

$$\begin{aligned} I_i &= \begin{cases} 1 & \text{if } \Delta_{(n-i+1):n}Y > \tilde{\theta}(i, \mathcal{G}_{i-1}, \mathcal{G}'_{i-1}) \\ 0 & \text{otherwise} \end{cases} & i &= 1, \dots, m \\ I'_i &= \begin{cases} 1 & \text{if } -\Delta_{i:n}Y > \tilde{\theta}(i, \mathcal{G}_i, \mathcal{G}'_{i-1}) \\ 0 & \text{otherwise} \end{cases} & i &= 1, \dots, m' \end{aligned} \quad (13)$$

While the threshold function $\tilde{\theta}(i, \mathcal{G}_a, \mathcal{G}'_b)$ has the following definition

$$\tilde{\theta}(i, \mathcal{G}_a, \mathcal{G}'_b) := \sqrt{\hat{\sigma}^2} \cdot \begin{cases} \theta(p; n, n) & \text{if } a = 0, b = 0 \\ \theta\left(p; n - \sum_{j=1}^a I_j, n - \sum_{j=1}^a I_j\right) & \text{if } a \neq 0, b = 0 \\ \theta\left(p; n - i + 1 - \sum_{j=1}^b I'_j, n - \sum_{j=1}^a I_j - \sum_{j=1}^b I'_j\right) & \text{if } a \neq b \text{ and } b \neq 0 \\ \theta\left(p; n - i + 1 - \sum_{j=1}^a I_j, n - \sum_{j=1}^a I_j - \sum_{j=1}^b I'_j\right) & \text{otherwise} \end{cases} \quad (14)$$

where $\hat{\sigma}^2$ indicates the sample variance estimator of $\{\Delta_1 Y, \dots, \Delta_n Y\}$ and $\theta(p; k, n')$ is computed according to the formulas in Eq. 10 and Eq. 11 given p .

Fixed a tolerance level $p \in [0, 1]$, the Order Statistic (OS) estimator is defined as follows

$$\hat{V}_{OS} = \sum_{i=1}^m (\Delta_{(n-i+1):n}Y)^2 \mathbb{1}_{\{\Delta_{(n-i+1):n}Y \leq \tilde{\theta}(i, \mathcal{G}_{i-1}, \mathcal{G}'_{i-1})\}} + \sum_{i=1}^{m'} (\Delta_{i:n}Y)^2 \mathbb{1}_{\{-\Delta_{i:n}Y \leq \tilde{\theta}(i, \mathcal{G}_i, \mathcal{G}'_{i-1})\}} \quad (15)$$

It should be noticed that, in the OS estimator formulation, each random variable corresponding to an increment of the process Y_t is compared with a suitable threshold that is updated according to the new information flow arrival, while $\hat{\sigma}^2$ is used to appropriately rescale the realization-varying threshold.

Basically, the algorithm which updates the information to define the thresholds starts from the maximum observation, then moves to the minimum observation, than removes towards the second largest realization and so on and so forth. The sequences $\{\mathcal{G}_i\}_{i=1}^m$ and $\{\mathcal{G}'_i\}_{i=1}^{m'}$ allow to take into account the

information history to update the thresholds and the introduction of the second sequence $\{\mathcal{G}'_i\}_{i=1}^{m'}$ has the goal of exploiting the property of symmetry of the Normal distribution in the definition of our new estimator. In the practical use of the estimator, it should be noticed that the observations should be half positive and half negative in order to avoid possible distortion, this is clearly coherent with the symmetric choice of the distribution.

To give an intuition of the behaviour of this new estimator, we propose hereafter a simplified setting. In Figure 1, possible realizations of Standard Normal random variables (blue segments) with their threshold levels (dashed lines) are shown in decreasing order. The third ordered observation is composed by a Gaussian realization with the addition of a small jump realization (red interval). The comparison between the second and the third ordered observations underlines the need for taking into account the frequency of the realizations as well as their sizes, in the jump detection procedure. Indeed, if a fixed threshold, corresponding for example to the maximum admissible value for Normal random variables, having set the tolerance level p , was used to discriminate observations contaminated by jumps or not, the third realization of Figure 1 would not be detected as jump. On the contrary, the use of realization-varying thresholds allows to identify this kind of realizations interested by a jump component. Roughly speaking, an unusually high frequency of observations near the second and the third greatest values of

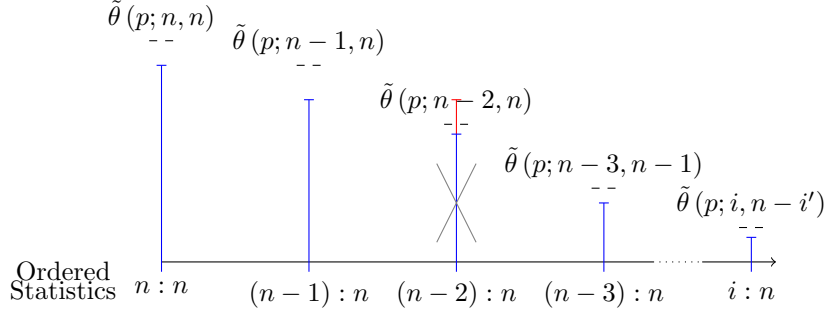


Figure 1: Some possible ordered realizations of Standard Normal random variables (in blue) with a jump component realization addition (in red) and their relative OS threshold levels (dashed line), in a simplified framework.

Algorithm 1: Base algorithm to compute the IV by means of the OS estimator.

Input: $(\Delta_{n:n}y, \dots, \Delta_{1:n}y)$ vector of ordered observations, p tolerance level, s^2 estimate of the sample variance of realizations

Output: s_{IV} IV estimate, (j_n, \dots, j_1) vector of boolean jump indicators associated to the vector $(\Delta_{n:n}y, \dots, \Delta_{1:n}y)$

Initialize $(j_n, \dots, j_1) = (0, \dots, 0)$, $n' = n$, $k = 1$, $k' = 1$;

for $i = n, n-1, \dots, \frac{n}{2}$ **do**

 Compute $\theta(p; n' - k + 1, n')$ according to Eq. 10 and Eq. 11 ;

 Evaluate $\tilde{\theta}_1 = \sqrt{s^2} \theta(p; n' - k + 1, n')$;

if $\Delta_{i:n}y > \tilde{\theta}_1$ **then**

$j_i \leftarrow 1$;

$n' \leftarrow n' - 1$;

else

$k \leftarrow k + 1$;

 Compute $\theta(p; n' - k' + 1, n')$ according to Eq. 10 and Eq. 11 ;

 Evaluate $\tilde{\theta}_2 = \sqrt{s^2} \theta(p; n' - k' + 1, n')$;

if $-\Delta_{(n-i+1):n}y > \tilde{\theta}_2$ **then**

$j_{n-i+1} \leftarrow 1$;

$n' \leftarrow n' - 1$;

else

$k' \leftarrow k' + 1$;

Evaluate $s_{IV} = \sum_{i=1}^n (\Delta_{i:n}y)^2 \cdot j_i$

the observations is interpreted by our estimator as a signal that these realizations cannot come from a Gaussian random variable. Obviously, our estimator is not able to disentangle which realization is really affected by a jump.

Moreover, for the sake of completeness, pure Gaussian realizations could also be detected as jumps by the OS estimator with a certain probability (whose maximum level is $p\%$).

This estimator is practically implemented by the simple iterative algorithm reported in Algorithm 1. For simplicity, as already stated, we consider the case of an even number of n observations.

3.6 Iterative Algorithm for Local Volatility Estimation

A further extension concerning the OS estimator is its application to an iterative algorithm in order to estimate the time-varying volatility of the Y_t process.

The estimation of the local volatility σ_t of the Y_t process is not completely straightforward and it involves an iterative two-step estimation procedure. At first, the process realizations must be renormalized by the corresponding local volatility estimates and, then, the OS estimator, including a kernel function, must be applied to such renormalized observation set, obtaining new time-varying volatility estimates. The formal definition is the following.

First of all, a kernel function with bandwidth h is defined as

$$K_h(s) := \frac{1}{h} K\left(\frac{s}{h}\right) \quad (16)$$

where $K(s)$ is a non-negative weighting function, i.e. such that $\int_{-\infty}^{+\infty} K(s) ds = 1$ and $K(s) \geq 0 \quad \forall s$.

Considering the iteration $j > 1$ and let $\left\{s_i^{(j)}\right\}_{i=1}^n$ be the j -th sequence of local volatility estimates associated to the record time of each random variable in the set $\{\Delta_1 Y, \dots, \Delta_n Y\}$, then we consider the j -th set of renormalized random variables

$$\left\{\Delta_i \bar{Y}^{(j)}\right\}_{i=1}^n := \left\{\Delta_i \bar{Y}^{(j)} : \Delta_i \bar{Y}^{(j)} = \frac{\Delta_i Y}{s_i^{(j)}} \text{ for } i = 1, \dots, n\right\} \quad (17)$$

Once named $\{\Delta_{n:n} \bar{Y}^{(j)}, \dots, \Delta_{1:n} \bar{Y}^{(j)}\}$ the ordered set of these variables, we introduce the function $f^{(j)}$ that maps the index i of each random variable in the ordered set $\{\Delta_{(n-i+1):n} \bar{Y}^{(j)}\}_{i=1}^n$ to the index $\tilde{i} = f^{(j)}(i)$ of the corresponding random variable in the set $\{\Delta_i \bar{Y}^{(j)}\}_{i=1}^n$.

The kernel OS estimator, for the j -th iteration, is defined as

$$\hat{\sigma}_{OS}^{2(j)}(t) = \frac{\sum_{i=1}^m K_{h,\tilde{i}}^t(\Delta_{(n-i+1):n} \bar{Y}^{(j)})^2 \max\left\{\mathbb{1}_{\{\Delta_{(n-i+1):n} \bar{Y}^{(j)} \leq \bar{\theta}(i, \bar{\mathcal{G}}_{i-1}^{(j)}, \bar{\mathcal{G}}'_{i-1}^{(j)})\}}, 1 - \bar{X}_{n-i+1}^{(j-1)}\right\} + \sum_{i=1}^{m'} K_{h,\tilde{i}}^t(\Delta_{i:n} \bar{Y}^{(j)})^2 \max\left\{\mathbb{1}_{\{-\Delta_{i:n} \bar{Y}^{(j)} \leq \bar{\theta}(i, \bar{\mathcal{G}}_i^{(j)}, \bar{\mathcal{G}}'_{i-1}^{(j)})\}}, 1 - \bar{X}_i^{(j-1)}\right\}}{\sum_{i=1}^n K_{h,i}^t \delta t} \quad (18)$$

where the sequences $\left\{\bar{\mathcal{G}}_i^{(j)}\right\}_{i=0}^m$ and $\left\{\bar{\mathcal{G}}'_i^{(j)}\right\}_{i=0}^{m'}$ are such that

$$\begin{aligned} \bar{\mathcal{G}}_0^{(j)} &= \emptyset & \bar{\mathcal{G}}_i^{(j)} &= \{\bar{I}_1^{(j)}, \dots, \bar{I}_i^{(j)}\} \\ \bar{\mathcal{G}}'_0^{(j)} &= \emptyset & \bar{\mathcal{G}}'_i^{(j)} &= \{\bar{I}'_1^{(j)}, \dots, \bar{I}'_i^{(j)}\} \end{aligned} \quad (19)$$

and $\bar{I}_i^{(j)}$ and $\bar{I}'_i^{(j)}$ are random variables progressively defined as

$$\begin{aligned} \bar{I}_i^{(j)} &= \begin{cases} 1 & \text{if } \Delta_{(n-i+1):n} \bar{Y}^{(j)} > \bar{\theta}(i, \bar{\mathcal{G}}_{i-1}^{(j)}, \bar{\mathcal{G}}'_{i-1}^{(j)}) \text{ or } \bar{X}_{n-i+1}^{(j-1)} = 1 \\ 0 & \text{otherwise} \end{cases} & i = 1, \dots, m \\ \bar{I}'_i^{(j)} &= \begin{cases} 1 & \text{if } -\Delta_{i:n} \bar{Y} > \bar{\theta}(i, \bar{\mathcal{G}}_i^{(j)}, \bar{\mathcal{G}}'_{i-1}^{(j)}) \text{ or } \bar{X}_i^{(j-1)} = 1 \\ 0 & \text{otherwise} \end{cases} & i = 1, \dots, m' \end{aligned} \quad (20)$$

with $\bar{X}_k^{(j-1)} := \begin{cases} \bar{I}_{n-f^{(j-1)}^{-1}(f^{(j)}(k))+1}^{(j-1)} & \text{if } f^{(j-1)}^{-1}(f^{(j)}(k)) \in \{n, \dots, \lfloor \frac{n}{2} \rfloor\} \\ \bar{I}'_{f^{(j-1)}^{-1}(f^{(j)}(k))}^{(j-1)} & \text{if } f^{(j-1)}^{-1}(f^{(j)}(k)) \in \{0, \dots, \lfloor \frac{n}{2} \rfloor\} \end{cases}$ and m, m' as specified

in Subsection 3.5.

The threshold function $\bar{\theta}(i, \bar{\mathcal{G}}_a^{(j)}, \bar{\mathcal{G}}'_b{}^{(j)})$ writes as

$$\bar{\theta}(i, \bar{\mathcal{G}}_a^{(j)}, \bar{\mathcal{G}}'_b{}^{(j)}) := \begin{cases} \theta(p; n, n) & \text{if } a = 0, b = 0 \\ \theta\left(p; n - \sum_{j=1}^a \bar{I}_j^{(j)}, n - \sum_{j=1}^a \bar{I}_j^{(j)}\right) & \text{if } a \neq 0, b = 0 \\ \theta\left(p; n - i + 1 - \sum_{j=1}^b \bar{I}'_j^{(j)}, n - \sum_{j=1}^a \bar{I}_j^{(j)} - \sum_{j=1}^b \bar{I}'_j^{(j)}\right) & \text{if } a \neq b \text{ and } b \neq 0 \\ \theta\left(p; n - i + 1 - \sum_{j=1}^a \bar{I}_j^{(j)}, n - \sum_{j=1}^a \bar{I}_j^{(j)} - \sum_{j=1}^b \bar{I}'_j^{(j)}\right) & \text{otherwise} \end{cases} \quad (21)$$

and the kernel weight $K_{h,\tilde{i}}^t := K_h(\tilde{i}\delta t - t)$ is the kernel value associated with the order statistic $\Delta_{i:n}\bar{Y}$.

Note that $f^{(j-1)^{-1}}(f^{(j)}(i))$ stands for the index of the ordered random variable of $(j-1)$ -th iteration corresponding to the ordered random variable with index i of the j -th iteration. The variables $\bar{X}_k^{(j-1)}$ $k = 1, \dots, n$ allow to take into account the observations that have already been detected as jumps in the previous iterations of the algorithm in order to exclude them from the volatility estimation of the current iteration.

Furthermore, the inclusion of kernel weights in the definition of this estimator allows to give different importance to the observations in the sample in accordance with their temporal proximity to the time instant at which the local volatility needs to be estimated.

In addition, once $\hat{\sigma}_{OS}^{2(j)}(t)$ has been computed for all $t \in \{0, \delta t, \dots, n\delta t = T\}$, the set $\left\{s_i^{(j-1)}\right\}_{i=1}^n$ can be updated with these new estimates and the estimator can be applied again to the new renormalized random variables.

As starting volatility estimates, the sample variance of the whole set $\{\Delta_1 Y, \dots, \Delta_n Y\}$ can be coupled to each random variable $\Delta_i Y$ for $i = 1, \dots, n$.

It is worth mentioning that, with respect to the first iteration ($j = 1$), the indicators $\bar{I}_i^{(1)}$ and $\bar{I}'_i^{(1)}$ are defined as

$$\begin{aligned} \bar{I}_i^{(1)} &= \begin{cases} 1 & \text{if } \Delta_{(n-i+1):n}\bar{Y}^{(1)} > \bar{\theta}(i, \bar{\mathcal{G}}_{i-1}^{(1)}, \bar{\mathcal{G}}'_{i-1}^{(1)}) \\ 0 & \text{otherwise} \end{cases} \quad i = 1, \dots, m \\ \bar{I}'_i^{(1)} &= \begin{cases} 1 & \text{if } -\Delta_{i:n}\bar{Y}^{(1)} > \bar{\theta}(i, \bar{\mathcal{G}}_i^{(1)}, \bar{\mathcal{G}}'_{i-1}^{(1)}) \\ 0 & \text{otherwise} \end{cases} \quad i = 1, \dots, m' \end{aligned} \quad (22)$$

and $\bar{X}_i^{(0)} = 0 \quad \forall i = 1, \dots, n$. All the other variables and parameters coincide with the ones previously stated.

Finally, it is worth noting that, in general, the kernel function is an even function (i.e. $K(s) = K(-s)$), nevertheless, in order not to use information time preceding the volatility calculation time, in our implementation of such estimator we use a one-sided kernel function, that is $K(s) \neq 0$ only for $s \leq 0$. Thus, without loss of generality, we assume that the kernel function can also be non-symmetrical.

More precisely, the weighting function that we use in our practical implementation of such estimator is $K_h(t_i - t) = \begin{cases} \frac{1}{h} & \text{if } |t_i - t| \leq (h+1)\delta t \quad \text{and} \quad t_i - t < 0 \\ 0 & \text{otherwise} \end{cases}$ for each $t_i \in \{0, \delta t, \dots, n\delta t = T\}$.

The iterative algorithm to compute the time-varying volatility of the Y_t process is reported in Algorithm 2.

An on-line version (in Python code) of such algorithm is also available on the website².

3.7 Further Observations

By some approximations, we establish a correspondence between the threshold estimator proposed in Eq. 3 and the OS estimator defined in Eq. 15. For practical purposes, this match can be employed to perform a fair comparison between these two estimators.

In detail, starting from the OS estimator defined in Eq. 15 and fixing the threshold level equal to $\tilde{\theta}(i, \mathcal{G}_a, \mathcal{G}'_b) \equiv \tilde{\theta} = \sqrt{\hat{\sigma}^2}\theta(\bar{p}; n, n)$ for all $i = 1, \dots, n$, we get that each observation in the sample $\{\Delta_1 y, \dots, \Delta_n y\}$ is compared with the maximum admissible value for the discrete increments of Y_t^c , having set the tolerance level \bar{p} .

This particular implementation of the OS estimator is comparable to the threshold estimator in Eq. 3

²<https://github.com/sigmaquadro/VolatilityEstimator>

Algorithm 2: Base iterative algorithm to compute the time-varying volatility of the Y_t process by means of the OS estimator.

Input: $(\Delta_1 y, \dots, \Delta_n y)$ whole sample vector, p tolerance level

Output: (s_1, \dots, s_n) vector of volatility estimates, (j_1, \dots, j_n) vector of boolean jump indicators associated to $(\Delta_1 y, \dots, \Delta_n y)$

Set each component of the vector (s_1^2, \dots, s_n^2) equal to the sample variance estimate of $(\Delta_1 y, \dots, \Delta_n y)$;

Set the vector of boolean jump indicators $(j_1, \dots, j_n) = (0, \dots, 0)$;

Compute the normalized vector $\bar{y} := (\Delta_1 \bar{y}, \dots, \Delta_n \bar{y})$ with $\Delta_i \bar{y} = \frac{\Delta_i y}{s_i}$;

Compute the kernel vector associated with \bar{y} ;

Order the vector \bar{y} and rearrange the kernel and boolean vectors in the same way;

repeat

 Update the vector of boolean jump indicators (j_1, \dots, j_n) according to Eq. 20;

for $t=1, \dots, n$ **do**

 Apply the kernel OS estimator defined in Eq. 18 to the vector \bar{y} using the rearranged kernel and boolean vector;

 Update s_t with the square root of estimate produced by the kernel OS estimator;

 Update the normalized vector \bar{y} using the new estimates (s_1, \dots, s_n) ;

until the identified jumps before and after the application of the estimator are the same;

with threshold function corresponding to $\theta(\delta t) = 2 \log \frac{1}{\delta t} \hat{\sigma}^2$ with δt chosen such that

$$\begin{aligned} \bar{p} &= \mathbb{P} \left(\max_{i=1, \dots, n} |W_{(i+1)\delta t} - W_{i\delta t}| > \sqrt{2\delta t \log \frac{1}{\delta t}} \right) \approx 2\mathbb{P} \left(\max_{i=1, \dots, n} (W_{(i+1)\delta t} - W_{i\delta t}) > \sqrt{2\delta t \log \frac{1}{\delta t}} \right) \\ &\quad \updownarrow \\ \bar{p} &= \mathbb{P} \left(\max_{i=1, \dots, n} |Z_i| > \sqrt{2 \log \frac{1}{\delta t}} \right) \approx 2\mathbb{P} \left(\max_{i=1, \dots, n} Z_i > \sqrt{2 \log \frac{1}{\delta t}} \right) \\ &\quad \updownarrow \\ &\quad \theta \left(\frac{\bar{p}}{2}; n, n \right) \approx \sqrt{2 \log \frac{1}{\delta t}} \end{aligned} \quad (23)$$

where $Z_i = \frac{W_{(i+1)\delta t} - W_{i\delta t}}{\sqrt{\delta t}} \sim N(0, 1) \quad \forall i = 1, \dots, n$. The approximation holds for large $\sqrt{2 \log \frac{1}{\delta t}}$ and its derivation is reported in Appendix A.2.

We use this correspondence between the two estimators in order to be able to produce their fair performance comparison in the simulation tests.

Moreover, employing a different c.d.f. in the order statistic computation involved in the OS estimator represents a further extension of such estimator.

Indeed, as previously mentioned, recognizing that all the formulas proposed in Subsection 3.5 hold substituting the c.d.f. of the Standard Normal random variable with a symmetric distribution, the OS estimator can be implemented also assuming that the increments of the continuous part of Y_t have a distribution different from the Normal one but still symmetric. For instance, assuming that their distribution is the t-Student one.

Obviously, this is just an observation and additional comments and details are not included in this paper.

4 Numerical and Empirical Tests

4.1 Simulation Tests

We evaluated the performances of the OS estimator by applying it on simulated samples coming from stochastic processes with either finite activity or infinite activity jump part.

More precisely, we simulated two different processes: the Merton process, having a jump part corresponding to a compounded Poisson Process (finite activity), and a process composed by the superposition of a

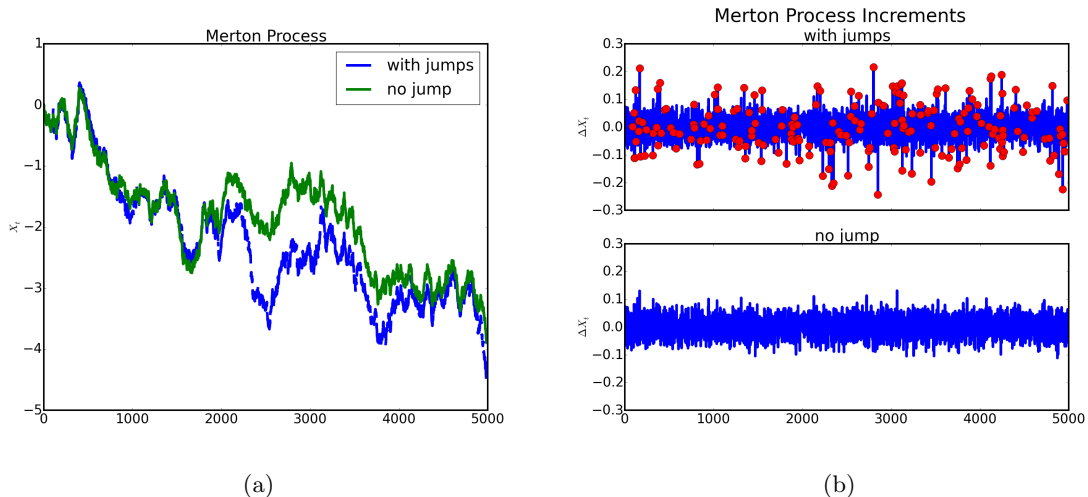


Figure 2: In the left panel, a Merton process simulated trajectory (blue line) and the corresponding diffusion-only trajectory (green line) are shown, while, in the right panel, the increment time series computed using such simulated trajectories are reported, respectively. The red dots stand for the true jump realizations. Model parameters: $b = 0$, $\sigma = 0.5$, $\lambda = 10$, $\delta = 1.5$ and $\mu = 0$. Simulation parameters: number of time-steps for each simulation $N_{TS} = 5000$, simulation time horizon $T = 20$.

Brownian motion and an independent Variance-Gamma (VG) process, having infinite activity jump part.

For all tests, we also compared the results concerning the jump detection obtained by the OS estimator with the ones produced by the threshold estimator. As previously explained, in order to make a fair comparison of these two estimators, we implemented the threshold estimator with threshold function stated in Subsection 3.7 and with δt calibrated in accordance with Eq. 23.

In practice, as far as the OS estimator is concerned, we used the iterative algorithm proposed in Subsection 3.6, while, with respect to the threshold estimator, we properly adapted the considered algorithm to the threshold estimator and we applied it.

We considered the following Merton model dynamics

$$\begin{cases} dX_t = bdt + \sigma dW_t + \gamma dN_t \\ X_0 = 0 \end{cases} \quad (24)$$

where W_t is a standard Brownian motion, σ is the volatility of the continuous part, N_t is a Poisson process with constant intensity λ and, conditionally on a jump occurring, γ is the jump size $\sim N(\mu, \delta^2)$ with mean μ and variance δ^2 . W_t and N_t are independent.

Chosen a parameter set (reported in the caption of the Figure 2 and 3), we simulated $M = 1000$ trajectories of such process and computed the relative increments, ΔX_t , in order to estimate the volatility σ for each path. We applied both the OS estimator and the threshold estimator to the increment time series and recorded the size of the realizations detected as jumps. As an example, Figures 2a and 2b show a Merton model trajectory and its increments, respectively. The corresponding jump detections performed by the OS estimator and the threshold estimator are reported in Figures 3a and 3b, respectively. The red dots stand for the realizations identified as jumps by the applied estimator.

Figure 4a shows the convoluted (i.e. including both the Brownian Motion and the pure jump realizations) jump size frequency distribution recreated from the simulated data provided by the two estimators considering all the samples. The peak in the OS cumulative jump size histogram is due to the error (of type I) in the jump detection that one is willing to accept fixing the tolerance level p . This behaviour is confirmed by the comparison between Figure 4a and Figure 4b where we show the convoluted jump size histogram obtained by applying the OS estimator to the same simulations cleaned-out from the Compounded Poisson process contributions. More precisely, in case of the application of the OS estimator on a rescaled Brownian motion increment time series, the error in the jump detection occurs in the $p\%$ of

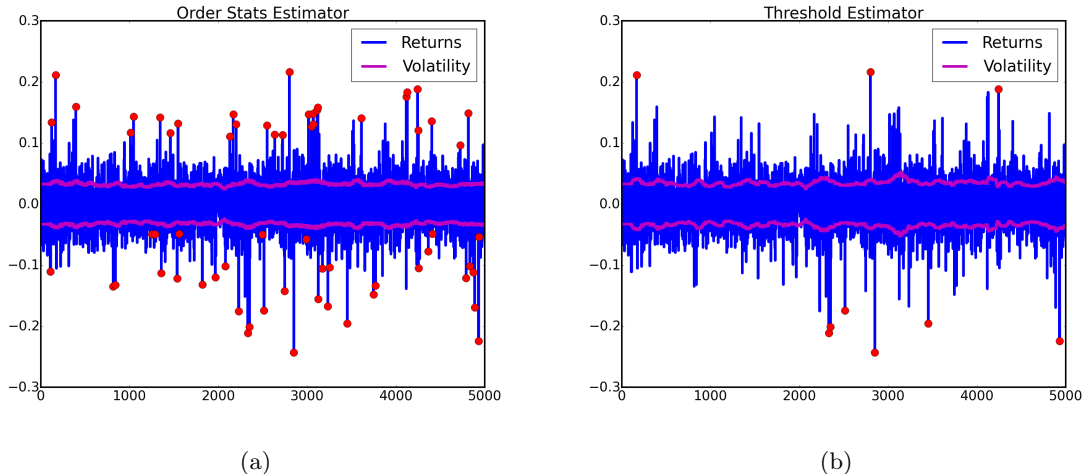


Figure 3: In the left panel, the detected jumps and the volatility estimates provided by the OS estimator on the Merton process simulated increment time series shown in Figure 2 are reported, while, in the right panel, the same outcomes provided by the threshold estimator are shown. Model parameters: $b = 0$, $\sigma = 0.5$, $\lambda = 10$, $\delta = 1.5$ and $\mu = 0$. Simulation parameters: number of time-steps for each simulation $N_{TS} = 5000$, simulation time horizon $T = 20$. Estimator parameters: OS estimator tolerance level $p = 5\%$, bandwidth $h = 100$.

cases with respect to the maximum (or the minimum, depending on the starting point, i.e. the maximum or the minimum of the ordered realizations, of the recursive algorithm in proposed in Subsection 3.6). In Figure 5 we report the observed probability when applying the OS estimator to a Gaussian noise. Contrarily to our expectations, the probability is not stuck and equal to p , but it decreases moving into the central region of the order statistics. This effect is essentially due to the fact that we are neglecting the correlation among ordered realizations when we compute Eq. 11. Despite this decrease of the probability, a peak around 0 is evident in Figure 4 and it is due to the higher probability of observing a realization around zero. As a consequence, even if the probability of committing an error of type I in the jump detection is smaller around zero, the number of misclassified realizations is quite high and this explains the presence of the peak.

To control this error, all realizations identified as jumps by the estimator that are smaller, in absolute value, than the estimated volatility were reclassified as ordinary observations. The new convoluted jump size histogram is presented in Figure 6. Such figure shows the threshold estimator limit in recognizing as non-Brownian realizations many jumps whose size is comparable with the one of the continuous part process increments (hidden jumps), while it shows as the OS estimator, based on order statistics, tries to reduce this bias. The area between the red and blue line represents the gain in the hidden jump identification produced by the OS estimator.

Moreover, starting from the empirical characteristic function (e.c.f.) of the cumulative jump size, we isolated the distribution of the pure jump size to provide a deeper comparison between the two estimator results. Figure 7 reports the obtained distributions and confirms the improvement produced by the OS estimator in the jump detection. The technique used to filter and isolate the jump size distribution from its convolution with the Gaussian distribution is described in Appendix B.1.

Finally, mean time-varying volatility estimates produced by the two estimators, obtained by averaging across the M simulations, are reported in Figure 8. As expected, the OS estimator produces volatility estimates nearer to the real volatility values, since it is capable of detecting jumps even when their size is comparable to the one of the realizations of the continuous part of the process.

For what concerns the infinite activity, the process composed by the sum of a Brownian motion and a VG process (VG+BM process) has the following dynamics

$$\begin{cases} dX_t = dX_t^c + dX_t^{VG} = \underbrace{bdt + \sigma dZ_t}_{dX_t^c} + \underbrace{\alpha dV_t + \beta dW_{V_t}}_{dX_t^{VG}} \\ X_0 = 0 \end{cases} \quad (25)$$

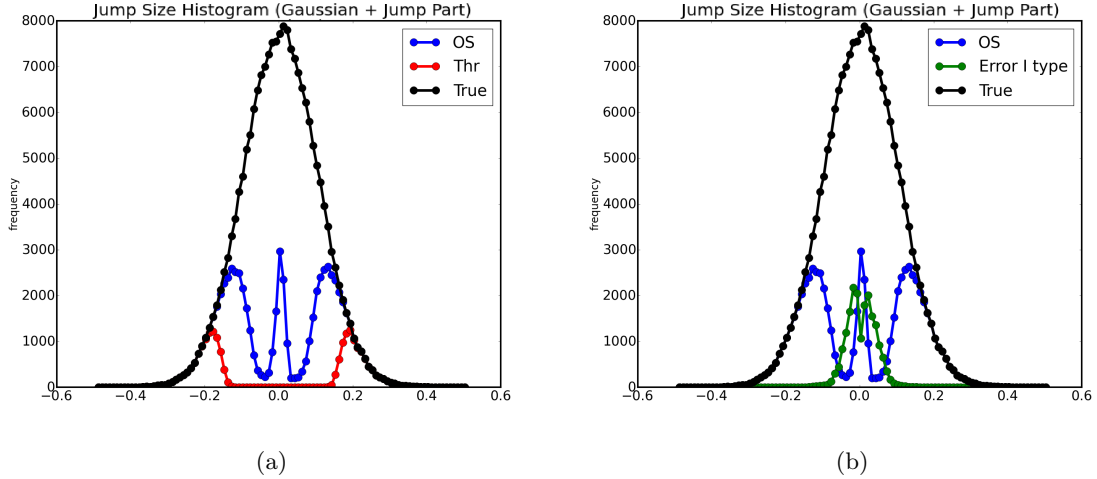


Figure 4: In the left panel, the cumulative jump size (i.e. including both the Brownian Motion and the pure jump realizations) histograms created using the realizations affected by true jumps (black line), the jump realizations identified by the OS estimator (blue line) and the ones identified by the threshold estimator (red line) are shown, while, in the right panel, the cumulative jump size histograms created using the jump realizations identified through the OS estimator application on the process increment time series cleaned out from the Compounded Poisson contributions is presented (green line), in addition to the previously described data. Model parameters: $b = 0$, $\sigma = 0.5$, $\lambda = 10$, $\delta = 1.5$ and $\mu = 0$. Simulation parameters: number of time-steps for each simulation $N_{TS} = 5000$, simulation time horizon $T = 20$, number of simulations $M = 1000$. Estimator parameters: OS estimator tolerance level $p = 5\%$, bandwidth $h = 100$.

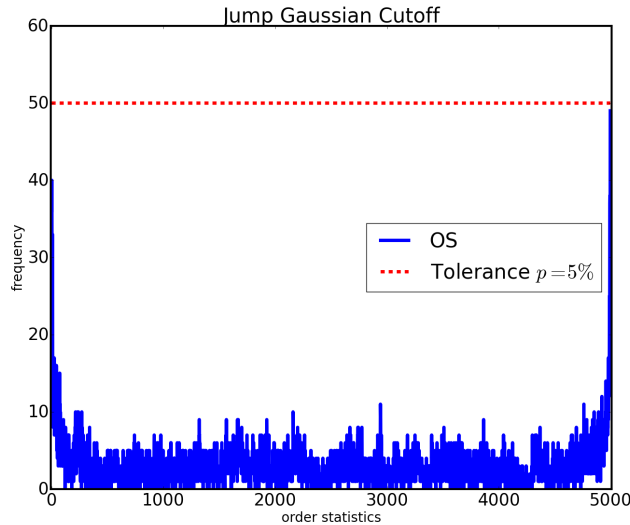


Figure 5: Frequency of the Gaussian realizations that are wrongly classified as jumps by the OS estimator (blue line) applied on the Merton process increment time series. The red dashed line stand for the maximum frequency of error of type I that the OS estimator can commit, i.e. $Mp = 50$. Model parameters: $b = 0$, $\sigma = 0.5$, $\lambda = 10$, $\delta = 1.5$ and $\mu = 0$. Simulation parameters: number of time-steps for each simulation $N_{TS} = 5000$, simulation time horizon $T = 20$, number of simulations $M = 1000$. Estimator parameters: OS estimator tolerance level $p = 5\%$, bandwidth $h = 100$.

where $V_t \sim \Gamma_t\left(\frac{1}{k}, \frac{1}{k}\right)$ is the Gamma subordinator process with variance kt and, thus, X_t^{VG} is a Variance-Gamma process with parameters α and β , while σ is the volatility of the continuous part process (X_t^c) and Z_t and W_t are two independent Brownian motions.

As in the Merton model case, we set the model parameters (as described in the caption of the Figure 9

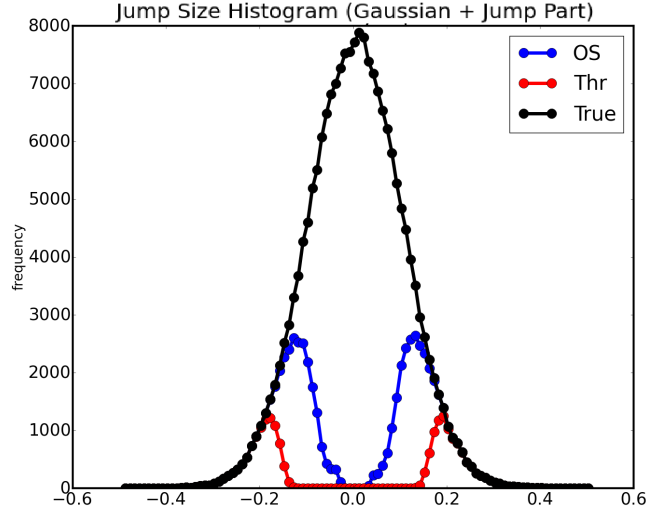


Figure 6: Cumulative jump size (i.e. including both the Brownian Motion and the pure jump realizations) histograms created using the realizations affected by true jumps (black line), the jump realizations identified by the OS estimator including the error of I type control (blue line) and the ones identified by the threshold estimator (red line). Model parameters: $b = 0$, $\sigma = 0.5$, $\lambda = 10$, $\delta = 1.5$ and $\mu = 0$. Simulation parameters: number of time-steps for each simulation $N_{TS} = 5000$, simulation time horizon $T = 20$, number of simulations $M = 1000$. Estimator parameters: OS estimator tolerance level $p = 5\%$, bandwidth $h = 100$. Note that the control on the error of I type corresponds to reclassifying all the realizations identified as jumps but with size in absolute value smaller than the estimated volatility as ordinary observations.

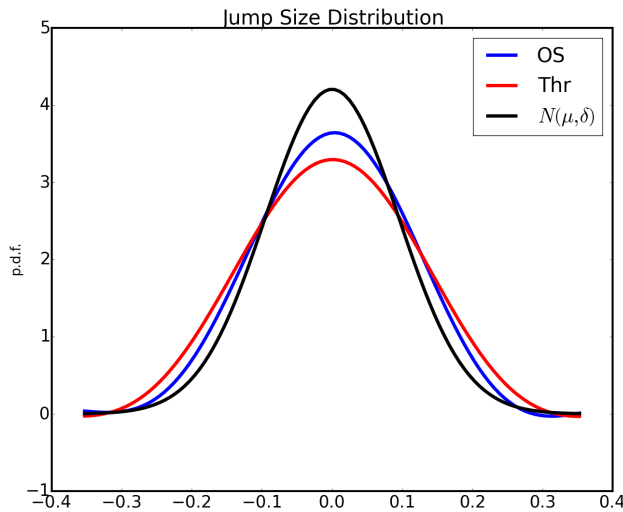


Figure 7: True jump size distribution (black line) and jump size distributions isolated from the cumulative ones obtained through the OS estimator (blue line) and the threshold estimator (red line) application on the simulated increment time series. Model parameters: $b = 0$, $\sigma = 0.5$, $\lambda = 10$, $\delta = 1.5$ and $\mu = 0$. Simulation parameters: number of time-steps for each simulation $N_{TS} = 5000$, simulation time horizon $T = 20$, number of simulations $M = 1000$. Estimator parameters: OS estimator tolerance level $p = 5\%$, bandwidth $h = N_{TS}$.

and 10), we simulated $M = 1000$ trajectories of such process and computed the relative increments ΔX_t in order to estimate the volatility σ . To the resulting time series we applied the two estimators obtaining the local volatility estimates.

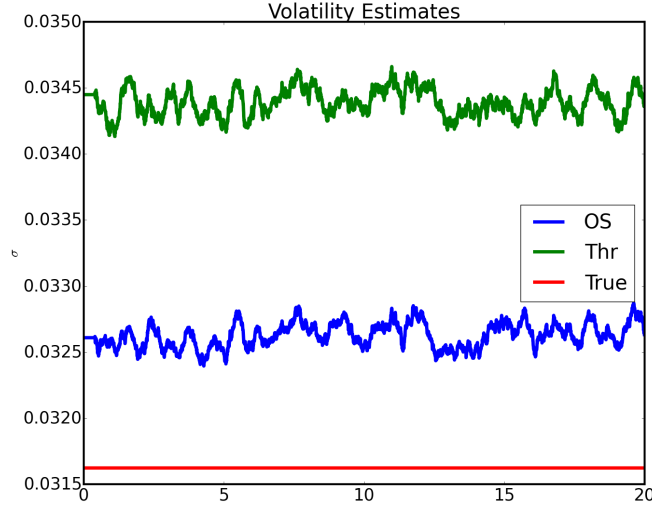


Figure 8: Comparison among the average time-varying volatility estimates provided by the OS estimator (blue line) and the threshold estimator (green line) application on the simulated Merton process increment time series and the true values (red line). Model parameters: $b = 0$, $\sigma = 0.5$, $\lambda = 10$, $\delta = 1.5$ and $\mu = 0$. Simulation parameters: number of time-steps for each simulation $N_{TS} = 5000$, simulation time horizon $T = 20$, number of simulations $M = 1000$. Estimator parameters: OS estimator tolerance level $p = 5\%$, bandwidth $h = 100$. Note that the true volatility value which must be compared with the estimates is $\sigma\sqrt{\Delta t}$ where, in our implementation,

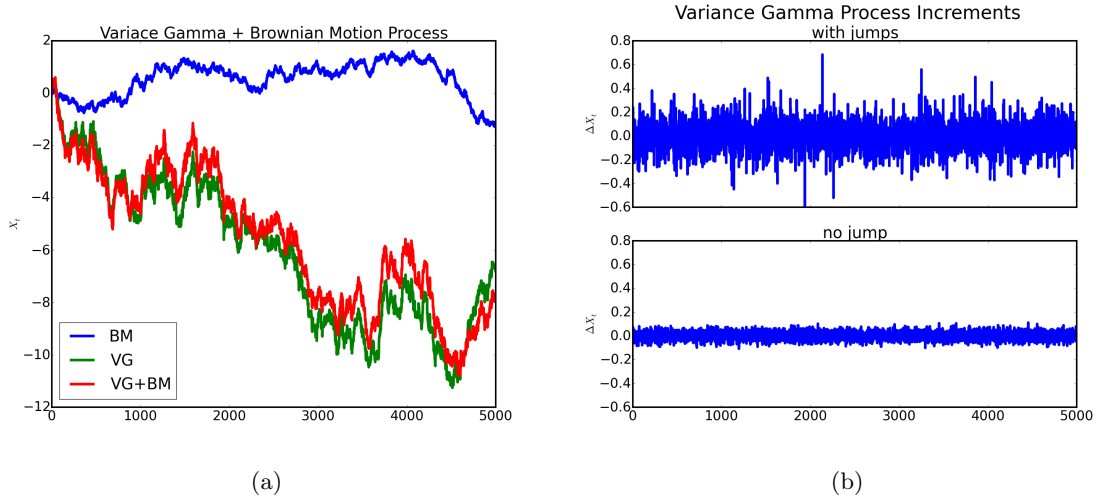
$$\Delta t = \frac{T}{N_{TS}} = 0.004.$$


Figure 9: In the left panel, a Variance-Gamma (VG) process simulated trajectory (green line), a Brownian motion (BM) simulated trajectory (blue line) and the trajectory resulting by their sum (VG+BM) (red line) are shown. In the right panel, the increment time series computed using the VG+BM and the BM simulated trajectories are reported, respectively. Model parameters: $b = 0$, $\sigma = 0.5$, $\alpha = 0$, $\beta = 1.5$ and $k = 0.004$. Simulation parameters: number of time-steps for each simulation $N_{TS} = 5000$, simulation time horizon $T = 20$.

As an example, Figures 9a and 9b show a trajectory of this model and its increments, respectively. While, the corresponding jump detections performed by the OS estimator and the threshold estimator are reported in Figures 10a and 10b, respectively. Moreover, the histograms of the realizations identified as jumps by the two different estimators across the simulations are reported in Figure 11a, while the corresponding jump size distributions isolated from the cumulative ones are shown in Figure 11b.

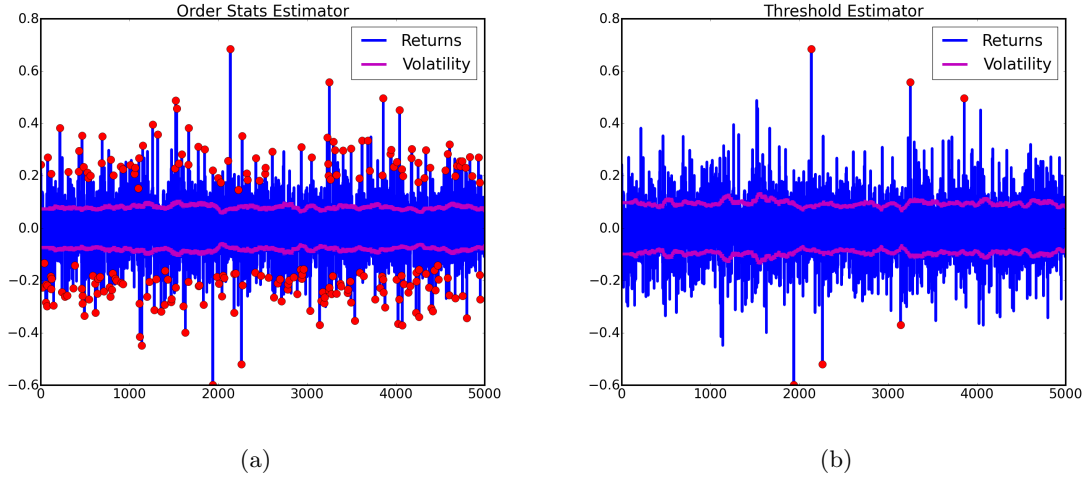


Figure 10: In the left panel, the detected jumps and the volatility estimates provided by the OS estimator on the VG+BM process simulated increment time series shown in Figure 9 are reported, while, in the right panel, the same outcomes provided by the threshold estimator are shown. Model parameters: $b = 0$, $\sigma = 0.5$, $\alpha = 0$, $\beta = 1.5$ and $k = 0.004$. Simulation parameters: number of time-steps for each simulation $N_{TS} = 5000$, simulation time horizon $T = 20$. Estimator parameters: OS estimator tolerance level $p = 5\%$, bandwidth $h = 100$.

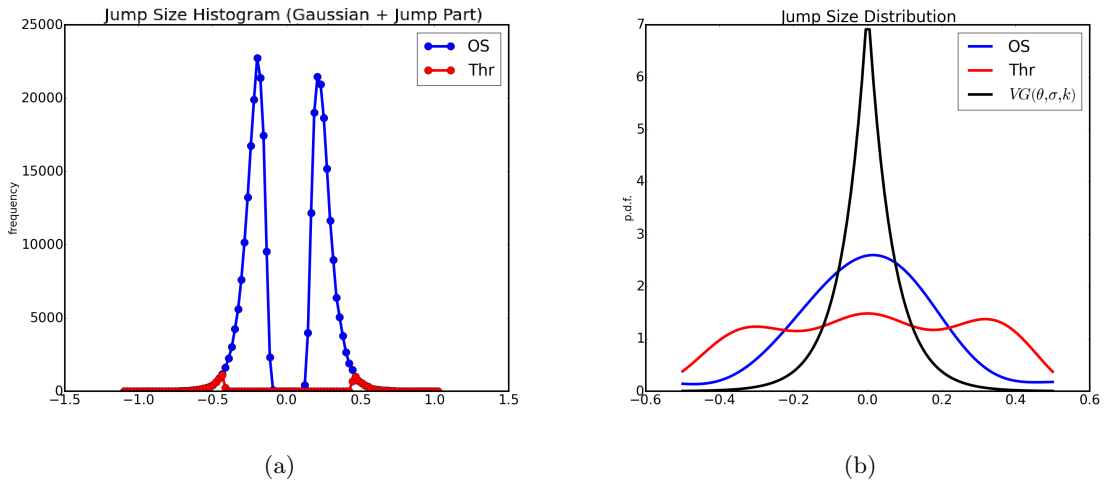


Figure 11: In the left panel, the detected jumps and the volatility estimates provided by the OS estimator on the VG+BM process simulated increment time series shown in Figure 9 are reported, while, in the right panel, the same outcomes provided by the threshold estimator are shown. Model parameters: $b = 0$, $\sigma = 0.5$, $\alpha = 0$, $\beta = 1.5$ and $k = 0.004$. Simulation parameters: number of time-steps for each simulation $N_{TS} = 5000$, simulation time horizon $T = 20$, number of simulations $M = 1000$. Estimator parameters: OS estimator tolerance level $p = 5\%$, bandwidth $h = N_{TS}$.

The volatility estimates obtained from the two estimators averaging across the M simulations are shown in Figure 12. As in the finite activity jump case, the OS estimator is able to identify a larger number of non-Brownian realizations and to produce better volatility estimates than the threshold one. Nevertheless, with this kind of process, the error in the volatility estimate is very high.

4.2 Real Data Examples

We also tested the performances of our estimator on real data samples. In detail, we applied the OS algorithm to estimate the local volatility on the daily log-return time series of the IBM stock. We compared the obtained results with the ones provided by the time-varying volatility estimation via

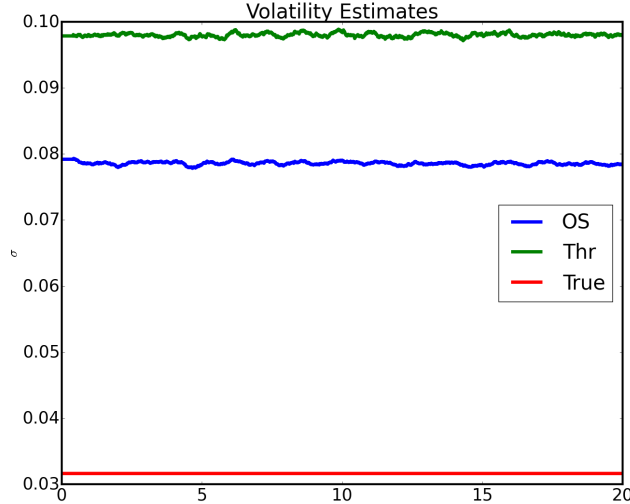


Figure 12: Comparison among the average time-varying volatility estimates provided by the OS estimator (blue line) and the threshold estimator (green line) application on the simulated Merton process increment time series and the true values (red line). Model parameters: $b = 0$, $\sigma = 0.5$, $\alpha = 0$, $\beta = 1.5$ and $k = 0.004$. Simulation parameters: number of time-steps for each simulation $N_{TS} = 5000$, simulation time horizon $T = 20$, number of simulations $M = 1000$. Estimator parameters: OS estimator tolerance level $p = 5\%$, bandwidth $h = 100$. Note that the true volatility value which must be compared with the estimates is $\sigma\sqrt{\Delta t}$ where, in our implementation, $\Delta t = \frac{T}{N_{TS}} = 0.004$.

GARCH model with t-Student innovations. For practical purposes, we used the demeaned time series. Figure 13 shows the volatility estimates provided by the OS estimator, while Figure 14 reports the GARCH volatility estimates. The red dots stand for the realizations identified as jumps by the OS estimator. Moreover, in Figures 13b, 13c the empirical c.d.f. of the whole sample renormalized realizations (red line), the empirical c.d.f. of the renormalized realizations identified as non-jumps by the OS estimator (blue line) and the Standard Normal random variable c.d.f. (black dashed line) are reported, both with linear and logarithmic scale. Instead, Figures 14b, 14c show the empirical c.d.f. of the whole sample (red line), the empirical c.d.f. of the GARCH residuals (blue line) and the c.d.f. of a t-Student random variable with degrees of freedom, location and scale parameters assumed for the GARCH model innovations (black dashed line), both with linear and logarithmic scale. Comparing Figure 13a with Figure 14a, the volatilities estimated by the OS estimator result smoother than the ones obtained by considering the GARCH model.

Moreover, it is worth noting that, in general, the OS estimated volatilities are smaller than the GARCH ones, since the former evaluates the Gaussian process volatility, filtering the detected jumps, while the latter provides an estimate of the whole process volatility.

5 Sanity Check: Empirical Results

In order to provide a sanity check for the OS estimator, we massively applied it on real data log-return times series and we tested whether the renormalized realizations classified as non-jumps really came from a standard Normal distribution as supposed by the OS estimator model.

5.1 Dataset Description and Diagnostic Procedure

The dataset used for the residual diagnostics consists of the S&P 500 stock daily log-return time series with more than 2000 observations in the period of interest from 1 January 2001 to December 2016, with a total of 307 time series. The stock log-returns were computed by using the close-prices.

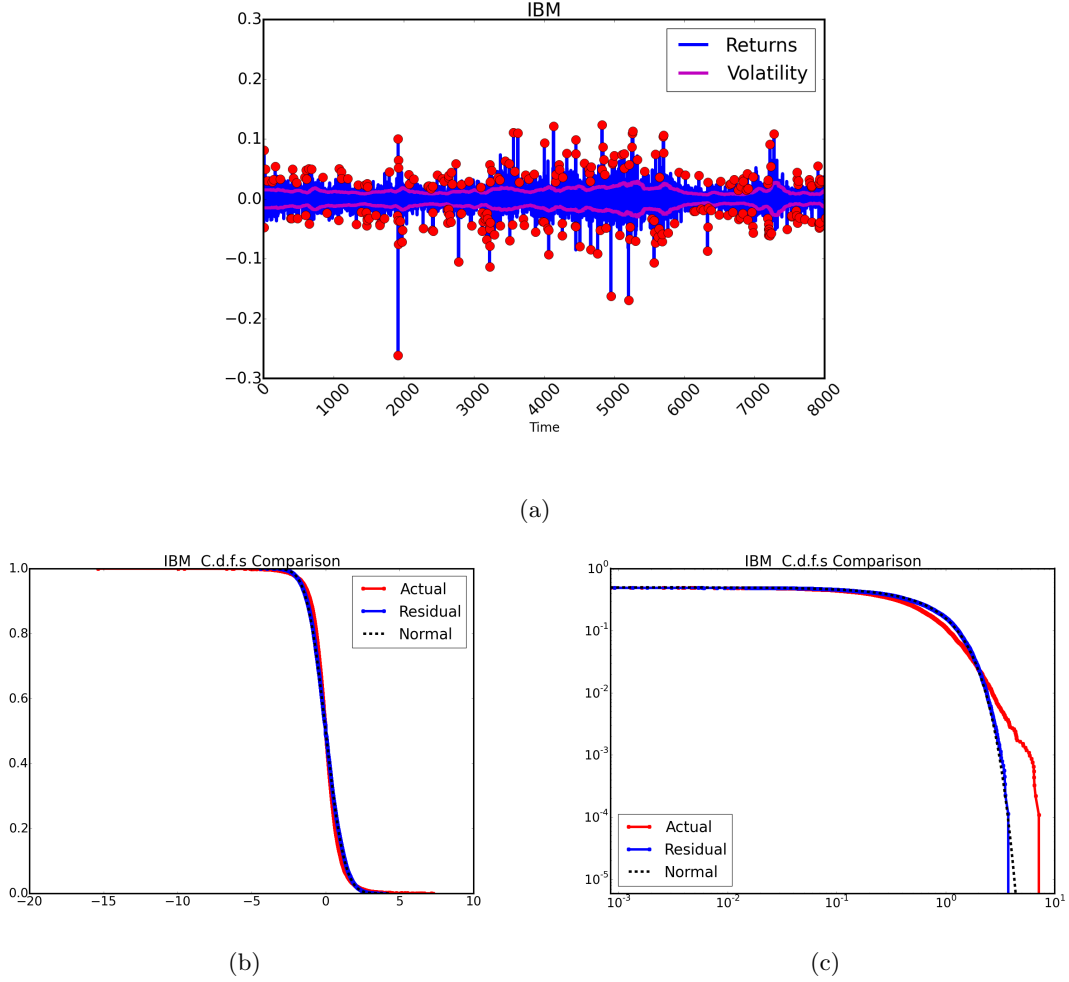


Figure 13: In the first panel (13a), the IBM stock daily log-return time series and the volatility estimate time series obtained by applying the OS estimator are reported. The red dots stand for the realizations identified as jumps by the OS estimator. While, in the other panels (13b and 13c), the empirical c.d.f. of the whole renormalized sample (red line), the empirical c.d.f. of the renormalized observations identified as non-jumps (blue line) and the c.d.f. of a Standard Normal random variable (black dashed line) are shown, in linear scale and logarithmic scale respectively. Time series parameters: number of observations $N = 9180$ (from 17 March 1980 to 9 August 2016), daily recording frequency. Estimator parameters: OS estimator tolerance level $p = 5\%$, bandwidth $h = 100$.

For each time series, we checked whether the renormalized realizations not classified as jumps by the OS estimator were distributed as a standard Normal random variable by applying the Anderson-Darling (AD) test. Roughly speaking, the AD test compares a theoretical distribution with an empirical one measuring their distance in an appropriate metric. If such distance is too large, then the null hypothesis that the analyzed sample comes from the theoretical distribution must be rejected. For further details about the AD test, refer to Anderson et al. (1954). We stress that in this case, as we are interested in proving the null hypothesis that the no-jump classified returns are Gaussian, the higher is the confidence level, the more severe the test is.

To provide strong evidences of the consistency check success, we set the confidence level of the AD test equal to 15%, allowing for a 15% of probability in the type I error occurrence (i.e. in the 15% of the cases we could reject the null hypothesis even if it was true).

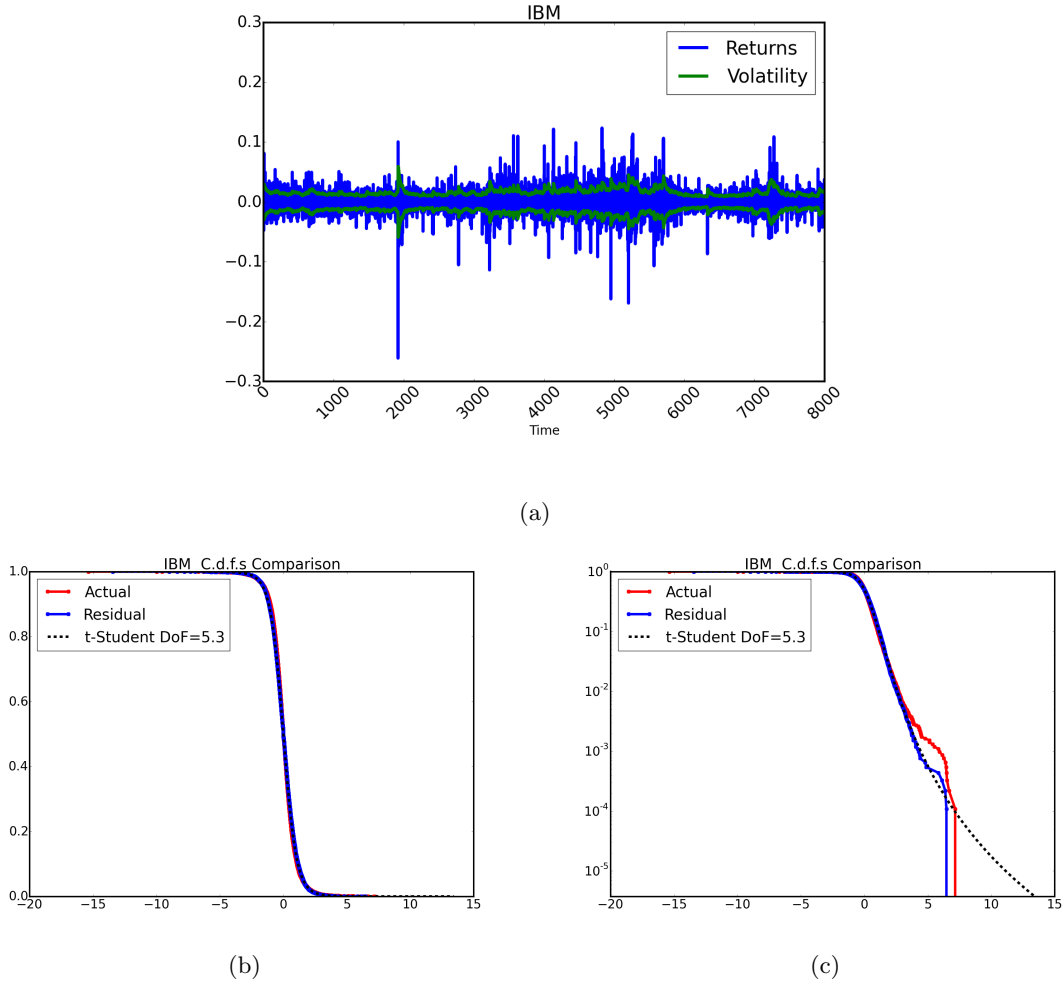


Figure 14: In the first panel (14a), the IBM stock daily log-return time series and the volatility estimate time series obtained by considering a GARCH model with T-Student innovations are reported. While, in the other panels (14b and 14c), the empirical c.d.f. of the whole sample (red line), the empirical c.d.f. of the GARCH residuals (blue line) and the c.d.f. of the T-Student random variable with degrees of freedom, location and scale parameters assumed for the GARCH model innovations (black dashed line) are shown, in linear scale and logarithmic scale respectively. Time series parameters: number of observations $N = 9180$ (from 17 March 1980 to 9 August 2016), daily recording frequency. Estimator parameters: GARCH model with symmetric T-Student innovations.

5.2 AD Test Results

The results of the application of the AD test with null hypothesis

$$H_0 : \text{the sample data comes from the Normal distribution}$$

on the 307 samples of the residuals classified as non-jumps are summarized in Table 1 (“Standard Prices” row).

The quite high percentage of time series for whom the null hypothesis of the AD test could not be rejected confirms the success of the performed consistency check. Nevertheless, in order to investigate the reasons leading to the rejection of the AD test null hypothesis for some times series, we carried out a deeper analysis on the log-return time series used as input in the consistency check.

As a result, we found out that, due to the quotation conventions, for some time series the frequency of exactly zero log-returns is much higher than expected, influencing the result of the AD test and implying the rejection of the null hypothesis.

More in detail, since 2001 the tick size (i.e. the minimum price increment in which the prices are quoted)

	# TS rejected H_0	Rejection Rate
Standard Prices	60	20%
Adjusted Prices	50	16%

Table 1: Number of time series that did not pass the AD test on the Normal distribution of the residuals classified as non-jumps and corresponding rejection rates. Time series features: daily residuals corresponding to the log-returns of the S&P 500 stocks classified as non-jumps by the OS estimator, number of observations $N > 2000$ (from 1 January 2001 to December 2016), 307 analyzed samples. Estimator parameters: OS estimator tolerance level $p = 5\%$, bandwidth $h = 50$.

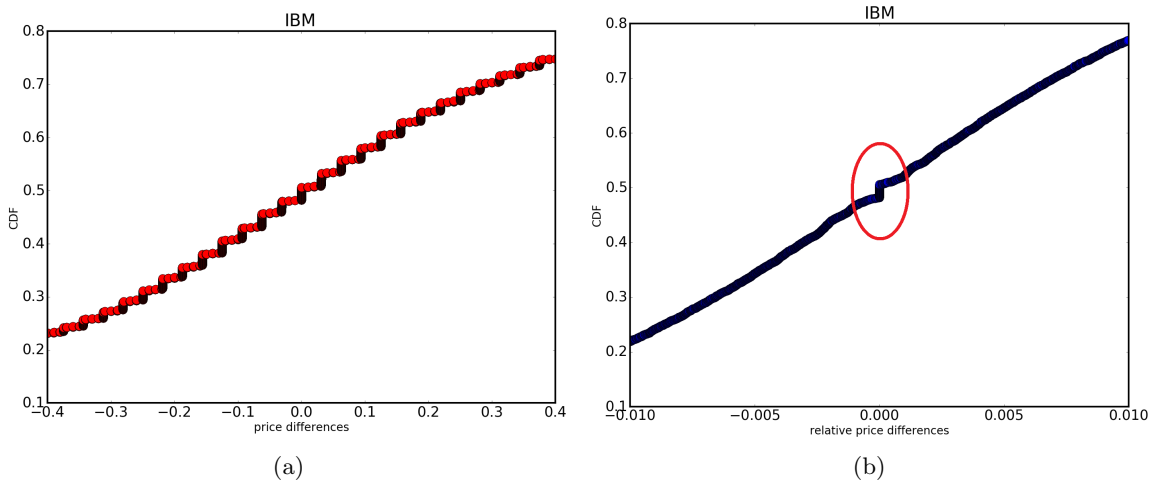


Figure 15: In the first panel (15a), the empirical c.d.f. of the IBM stock daily price difference time series is reported. While, in the second panel (15b), the empirical c.d.f. of the IBM stock daily relative return time series is shown. Time series parameters: observations from 3 September 1980 to 12 September 2012, daily recording frequency.

in the U.S. stock market has been 0.01\$. Consequently, the stock price differences suffer from a discretization issue and can only take values in the set of the multiples of 0.01 (i.e. $M = \{m : m = 0.01z, z \in \mathbb{Z}\}$), without spanning the interval $]m, m - 0.01[$ for each possible multiple $m \in M$. For instance, Figure 15a shows the empirical c.d.f. of the IBM stock price differences and the resulting step function is a clear signal of the discretization effect induced by the quotation convention.

With the relative return computation, the discrete price differences are divided by the corresponding previous stock prices. However, while the price differences exactly equal to zero stay to zero even if divided by the previous stock price (whatever its value is), all the other discrete price differences lead to real numbers whose values also depend on the (random) previous stock price amounts. As a result, the frequency of the relative returns exactly equal to 0 is higher than expected. As an example, Figure 15b shows the empirical c.d.f. of the relative returns of the IBM stock and the huge vertical step centered in zero is the outcome of the too high frequency of zero returns that can be probably caused by the price discretization effect. Except for zero, the empirical c.d.f. of the other returns results smooth.

The log-returns, being approximations of the relative returns, suffer from the same issue.

Adjusting the stock prices by completing them with random digit sequences leads to a slightly improvement of the AD test performances as reported in Table 1 (“Adjusted Prices” row).

For completeness, it should be mentioned that before 2001 the tick size typical of the U.S. stock market was $\frac{1}{8}\$ = 0.125\$$ (or other fractions) and thus the procedure to adjust these prices with random digits result slightly more tricky than adjusting the prices based on the decimal system quotation convention. To summarize, the analyzes confirm the overall agreement between the estimator reference distribution hypothesis and the empirical results.

6 Jumping VaR Model

The Order Statistic (OS) volatility estimator has a practical application in the field of Market Risk modeling. Indeed, it can be used as tool to improve the historical simulation method for VaR forecasting.

First of all, the volatility estimates can be employed to filter (re-normalize) the loss process random variables in order to make them identically distributed from the second moment point of view. Moreover, the distinction between the jump component and the ordinary (Gaussian) component realizations of the loss process identified through the estimator can be used to study jump probabilities and, therefore, to make a more accurate VaR prediction.

Given the sequence $\{l_i\}_{i=1}^N$ of the N realizations of the loss process from time $t-1$ to time $t-N-1$, the OS estimator allows to associate a boolean indicator stating the occurrence of a jump or not with each l_i . Formally, we define $\{j_i\}_{i=1}^N = \{j_1, j_2, \dots, j_N\}$ to be the sequence of the N indicators concerning the realizations of the jump component of the loss process from time $t-1$ to time $t-N-1$, with

$$j_i = \begin{cases} 1 & \text{if a jump occurs} \\ 0 & \text{otherwise} \end{cases} \quad \forall i = 1, \dots, N.$$

This additional information on the loss process up to time $t-1$ is thus exploited to produce a better estimate of the Value at Risk at time t .

The new model descriptions and the outcomes of their application are presented as follows.

6.1 Normalized Risk Model

The Normalized Risk model is the easiest model among the proposed ones. It is based on the assumption that the loss process random variables are independent but not identically distributed. Within this framework, in order to consider the loss process realizations drawn from i.i.d. random variables, they are renormalized by their standard deviations.

Given the sequence of the N realizations $\{l_i\}_{i=1}^N$ defined before and used to approximate the c.d.f. of the loss process at time t , let $\{\sigma_i\}_{i=1}^N$ be the volatility estimates associated with each realization of the loss process from time $t-1$ to time $t-N-1$. Under the hypothesis of zero-mean loss process random variables, the filter

$$\hat{l}_i = \frac{l_i}{\sigma_i} \quad \forall i = 1, \dots, N \quad (26)$$

makes these realizations drawn from i.i.d. random variables $\sim d(0, 1)$, where d is a generic distribution with zero mean and standard deviation equal to one.

The Value at Risk at time t with confidence level λ , $VaR_{\lambda,t}$, is computed as the sample λ -quantile of the empirical c.d.f. of the renormalized loss process at time t , built associating an uniform occurrence probability with each value \hat{l}_i , multiplied by the last disposable volatility σ_N , as we assumed that the last available volatility is the best forecast of the volatility over the VaR time horizon.

6.2 Jumping VaR Model

Supposing the loss process can be decomposed into an ordinary component and a jump one, the Jumping VaR model assumes that the occurrence or not of a jump at time t can be described by a Bernoulli random variable whose probability value is estimated by using the past realizations of the loss process (from time $t-1$ to time $t-T$, for a fixed time interval T).

The jump size is assumed independent on the past realizations of the jump component.

More precisely, let X_t be a Bernoulli random variable that assumes value 1 if a jump occurs at time t with probability $p_J(t)$ and 0 otherwise, associated with the corresponding loss process random variable. Formally,

$$X_t = \begin{cases} 1 & p_J(t) \\ 0 & 1 - p_J(t) \end{cases} \quad \forall t \quad (27)$$

with X_t, X_s independent $\forall t \neq s$.

The probability $p_J(t)$ is defined as a deterministic function of time only.

Within this framework, the occurrence probabilities p_i $i = 1, \dots, N$ associated with the N renormalized realizations of the loss process, $\{\hat{l}_i\}_{i=1}^N$, are computed as follows.

6.2.1 Occurrence Probabilities

Let $J = \{j_i \in \{j_i\}_{i=1}^N : j_i = 1\}$ be the set of the boolean indicators corresponding to a jump realization of the loss process from time $t-1$ to time $t-N-1$ and let $NOJ = \{j_i \in \{j_i\}_{i=1}^N : j_i = 0\}$ be the set of the boolean indicators corresponding to no jump realization of the loss process from time $t-1$ to time $t-N-1$. Under the model assumptions, the occurrence probabilities $p_i = \frac{\alpha}{N}$ assigned to the indicators in the set J and thus to the corresponding loss process realizations, are determined imposing that their sum is equal to the jump probability at time t , $p_J(t)$. Formally,

$$\begin{aligned} p_J(t) = \sum_{i=1}^{\#J} \frac{\alpha}{N} &\iff p_J(t) = \alpha \sum_{i=1}^{\#J} \frac{1}{N} \\ &\iff \alpha = \frac{p_J(t)}{p_J} \end{aligned} \quad (28)$$

The last equality follows from the definition of the quantity $p_J := \sum_{i=1}^{\#J} \frac{1}{N} = \frac{1}{N} \sum_{i=1}^N j_i = \frac{\#J}{N}$. Under the hypothesis of jump sizes independent on the past, the same occurrence probability is associated to all the jump indicators in the set J . The realizations of the loss process due to a jump are indeed considered equiprobable.

The occurrence probabilities $p_i = \frac{\beta}{N}$ assigned to the jump indicators in the set NOJ are computed requiring that all the occurrence probabilities p_i sum to 1

$$\begin{aligned} \sum_{i=1}^N p_i = 1 &\iff \sum_{i=1}^{\#J} \frac{\alpha}{N} + \sum_{i=1}^{\#NOJ} \frac{\beta}{N} = 1 \\ &\iff \alpha p_J + \beta (1 - p_J) = 1 \\ &\iff \beta = \frac{1 - \alpha p_J}{1 - p_J} = \frac{1 - p_J(t)}{1 - p_J} \end{aligned} \quad (29)$$

6.2.2 Jump Probability Forecasting

The previously defined sequence $\{j_i\}_{i=1}^N$ represents the realizations of the Bernoulli random variables X_s $s = t-1, \dots, t-N-1$. Using them and fixed a time interval of size $T \leq N$, the time-average jump probability within the interval from $s-T$ to s can be estimated through the estimator

$$\widehat{p_J(s)} = \frac{1}{T} \sum_{v=s-T}^s X_v \quad (30)$$

for each time $s \in \{t-1, \dots, t-(N+T+1)\}$.

It is worth noting that $\widehat{p_J(s)}$ produces an unbiased estimate of the time-average jump probability within the interval from $s-T$ to s (i.e. $\mathbb{E}[\widehat{p_J(s)}] = \frac{1}{T} \sum_{v=s-T}^s p_J(v)$). We also assume that the best forecast of the jump probability at time t given all the information up to time $t-1$ is the estimate of the time-average jump probability at time $t-1$.

6.2.3 $VaR_{\lambda,t}$ Computation

Fixed time t and knowing the realizations of the jump component from time $t-1$ to time $t-N-1$, the occurrence probabilities p_i $i = 1, \dots, N$ associated with the jump boolean indicators, $\{j_i\}_{i=1}^N$, and thus

with the corresponding renormalized loss process realizations, $\{\hat{l}_i\}_{i=1}^N$, are computed as explained in the Subsections 6.2.1, 6.2.2. The c.d.f. of the filtered loss process at time t is approximated assigning at each realization \hat{l}_i $i = 1, \dots, N$ the relative occurrence probability p_i $i = 1, \dots, N$. The $VaR_{\lambda,t}$ is estimated as the λ -quantile of this distribution multiplied by the last disposable volatility σ_N .

7 VaR Back-testing Performances

To practically test the goodness of the models proposed in Section 6, we forecast the Value at Risk for the 307 S&P500 stock log-return time series, assessing the back-testing outcomes.

More in detail, we compared the performance of 5 models:

- the filtered Jumping VaR model (FVaRjj), as presented in Section 6.2
- the (filtered) Normalized Risk model (FVaR)
- the standard historical simulation VaR using a sample made by 1000 realizations (HVaR)
- the standard historical simulation VaR using a sample made by 250 realizations (HVaR_250) and
- the performance of the filtered historical simulation method with GARCH model (t-Student innovations) volatility estimates (GARCH).

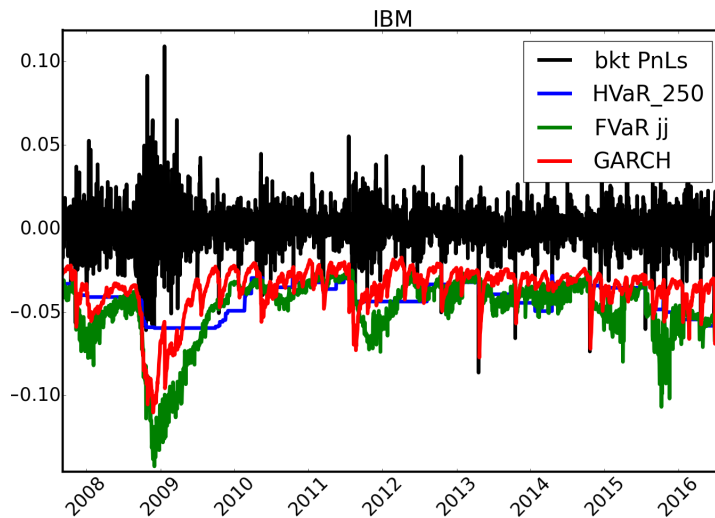


Figure 16: IBM stock daily log-return time series and corresponding VaR predictions implied by the Jumping VaR model (green line), the standard historical simulation method with 250-day time window (blue line), the filtered historical simulation method with T-GARCH volatility estimates (red line). Jumping VaR model parameters:

$T = 60$, $N = 250$. Estimator parameters: OS estimator tolerance level $p = 5\%$, bandwidth $h = 100$.

Figure 16 shows an example of the different VaR predictions for the IBM stock log-return time series (for sake of clarity, in this case we excluded the HVaR model from the plot).

In order to evaluate the goodness of the VaR models, we carried out a test involving the comparison between the daily back-testing log-returns and the predicted log-return distributions. For sake of clarity, the back-testing log-return is the log-return that effectively occurred at a fixed time t , while the predicted log-return distribution is the distribution predicted at time $t - 1$ for time t and used for the VaR forecast at time t .

For each time series and for each disposable date, the daily back-testing log-return was compared to the predicted log-return distribution and, assuming (null hypothesis) that the back-testing log-return is a realization of the predicted log-return distribution, the percentile rank corresponding to the considered

quantile was computed.

If the null hypothesis held, the value of each obtained percentile rank would be a realization of an Uniform $[0, 1]$ random variable. This backtesting approach is similar to the fundamental framework exploited in order to define the Anderson-Darling test, where two distributions are compared. To test this hypothesis, we compared the empirical c.d.f., resulting from the occurred percentile ranks, and the theoretical Uniform c.d.f..

Figure 17 shows the average absolute differences between the resulting empirical c.d.f. points and the Uniform c.d.f. for all the samples concerning the 307 S&P500 stock log-return time series.

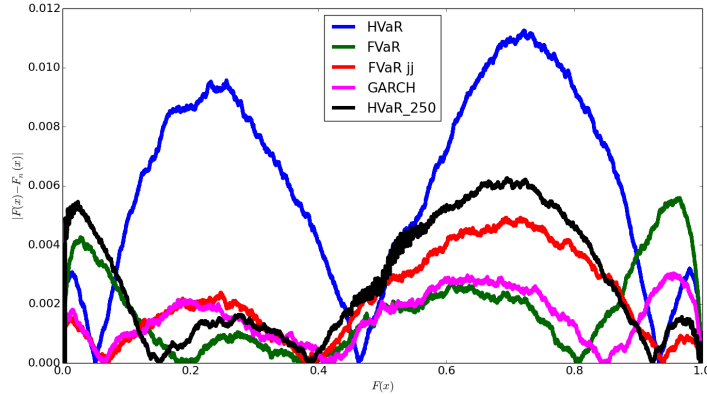


Figure 17: Absolute differences between the empirical c.d.f., resulting from the percentile ranks obtained comparing the daily back-testing log-returns and the predicted log-return distributions, and the theoretical Uniform c.d.f. for the S&P500 stock log-return time series. VaR models: standard historical simulation method (HVaR with time window of 1000 observations and HVaR_250 with time window of 250 observations), Normalized Risk model (FVaR), Jumping VaR model (FVaR jj), filtered historical simulation method with T-GARCH (GARCH model with T-Student innovations) volatility estimates (GARCH).

As far as the equity time series are concerned, the historical simulation methods, both with the time window of 1000 observations (HVaR) and with the time window of 250 observations (HVaR_250), have the worst performances, even if the reduction of the time window length improves the outcomes of this method for the VaR estimation. The performances of the Normalized Risk model (FVaR) are slightly better than the other models in the central part of the distribution that should correspond to the Gaussian regime of the true loss distribution. Nevertheless, the introduction of the jump adjustment involved by the Jumping VaR model (FVaR jj) allows to improve the performance of this method in the tails of the true loss distribution. Finally, the filtered historical simulation method with T-GARCH volatility estimates shows a performance comparable to the Jumping VaR model one.

8 Summary and Conclusion

We propose a new integrated variance estimator that relies on a well-defined theoretical framework of integrated variance threshold estimators and that allows to define a new time-varying volatility estimator for return time series. Our approach is based on the order statistics theory which enables to discriminate the jump part realizations from the continuous part ones of a stochastic process not only according to the size of the realizations, but also according to their frequency of occurrence.

Numerical and empirical examples compare the OS volatility estimator performances with the ones of the threshold and T-GARCH estimators, showing the capability of this estimator of disentangling the process volatility due to its continuous part from the further “volatility” due to the jump component.

An on-line version of the Python code implementing our estimator is also available on the website³.

The main advantages of the OS volatility estimator are the following.

- A formal definition of *jump* is provided and a jump classification algorithm is described.

³<https://github.com/sigmaquadro/VolatilityEstimator>

- The jump classification method is based on the definition of a confidence interval instead of a threshold. This allows the identification of hidden jumps, i.e. the jumps below the threshold.
- Only the Gaussian part of the volatility is estimated. This point can be helpful in order to calibrate a model where a stochastic differential equation, composed by a Wiener process and a jumping component, is specified (e.g. Local Stochastic Volatility Pricing Models).

Finally, we introduce a new and parsimonious Jumping VaR model for the Value at Risk predictions to include jump effects in the standard historical (filtered) VaR estimation framework. Empirical back-testing results on equity time series show that the Jumping VaR model outperforms the standard historical simulation method and gives comparable results to further advanced historical simulation methods.

The main advantages related to the Jumping VaR methodology are:

- specific assumptions on the tails of the returns distribution are not required (it is only required an assumption on the central part of the distribution), differently to GARCH-like models where an explicit assumption on innovators distribution is compulsory;
- thanks to the jump classification method, an ad-hoc methodology for the tail risk can be developed

A Volatility Estimator

A.1 Threshold $\theta(p; n, n)$ and $\theta(p; k, n')$ Derivation

Considering the framework introduced in Subsection 3.2, the threshold value $\theta(p; n, n)$ in Eq. 8 is computed as follows.

$$\begin{aligned}
\mathbb{P}\left(\max_{i=1, \dots, n} (W_{(i+1)\delta t} - W_{i\delta t}) > \theta^W(p; n, n)\right) &= p \iff \mathbb{P}\left(\max_{i=1, \dots, n} \frac{(W_{(i+1)\delta t} - W_{i\delta t})}{\sqrt{\delta t}} > \frac{\theta^W(p; n, n)}{\sqrt{\delta t}}\right) = p \\
&\iff \mathbb{P}\left(\max_{i=1, \dots, n} Z_i > \frac{\theta^W(p; n, n)}{\sqrt{\delta t}}\right) = p \\
&\iff \mathbb{P}\left(Z_{n:n} > \frac{\theta^W(p; n, n)}{\sqrt{\delta t}}\right) = p \\
&\iff \mathbb{P}\left(Z_{n:n} \leq \frac{\theta^W(p; n, n)}{\sqrt{\delta t}}\right) = 1 - p \\
&\iff F_{Z_{n:n}}\left(\frac{\theta^W(p; n, n)}{\sqrt{\delta t}}\right) = 1 - p \\
&\iff \theta^W(p; n, n) = \sqrt{\delta t} \underbrace{F_{Z_{n:n}}^{-1}(1 - p)}_{=: \theta(p; n, n)}
\end{aligned} \tag{31}$$

where Z_i are i.i.d. $\sim N(0, 1)$ for $i = 1, \dots, n$ and $Z_{n:n} := \max_{i=1, \dots, n} Z_i$, $F_{Z_{n:n}}(x) = (\Phi(x))^n$ is the cumulative distribution function (c.d.f.) of the maximum of n Standard Normal random variables and $\Phi(x)$ is the c.d.f. of a Standard Normal.

Repeating the same reasoning, the threshold value $\theta(p; k, n')$ in Eq. 10 is the following.

$$\begin{aligned}
&\mathbb{P}(k\text{-th ordered statistic in the dataset } \{(W_{(i+1)\delta t} - W_{i\delta t})\}_{i=1}^{n'} > \theta^W(p; k, n')) = p \\
&\iff \\
&\mathbb{P}(k\text{-th ordered statistic in the dataset } \left\{\frac{(W_{(i+1)\delta t} - W_{i\delta t})}{\sqrt{\delta t}}\right\}_{i=1}^{n'} > \frac{\theta^W(p; k, n')}{\sqrt{\delta t}}) = p \\
&\iff \\
&\mathbb{P}(k\text{-th ordered statistic in the dataset } \{Z_i\}_{i=1}^{n'} > \frac{\theta^W(p; k, n')}{\sqrt{\delta t}}) = p \\
&\iff \\
&\mathbb{P}(Z_{k:n'} > \frac{\theta^W(p; k, n')}{\sqrt{\delta t}}) = p \\
&\iff \\
&\mathbb{P}(Z_{k:n'} \leq \frac{\theta^W(p; k, n')}{\sqrt{\delta t}}) = 1 - p \\
&\iff \\
&F_{Z_{k:n'}}\left(\frac{\theta^W(p; k, n')}{\sqrt{\delta t}}\right) = 1 - p \\
&\iff \\
&\theta^W(p; k, n') = \sqrt{\delta t} \underbrace{F_{Z_{k:n'}}^{-1}(1 - p)}_{=: \theta(p; k, n')}
\end{aligned} \tag{32}$$

where $F_{Z_{k:n'}}(x)$ is the c.d.f. of the k -th order statistic in dataset of n' Standard Normal random variables. According to the order statistic theory (David et al. (2003))

$$\begin{aligned}
F_{Z_{k:n'}}(x) &= I_{\Phi(x)}(k, n' - k + 1) \\
&= \frac{n!}{(k-1)!(n-k)!} \int_0^{\Phi(x)} u^{k-1} (1-u)^{n-k} du
\end{aligned} \tag{33}$$

with $\Phi(x)$ c.d.f. of a Standard Normal and $I_x(a, b)$ Incomplete Beta function with parameters a, b .

A.2 Approximation $\mathbb{P}\left(\max_{i=1, \dots, n} |Z_i| > \Lambda\right) \approx 2\mathbb{P}\left(\max_{i=1, \dots, n} Z_i > \Lambda\right)$ Derivation

Let $Z_i \stackrel{\text{i.i.d.}}{\sim} N(0, 1)$ for $i = 1, \dots, n$, let $F_Z(z) = \Phi(z)$ be the c.d.f. of a Standard Normal random variable and let $\Lambda \in \mathbb{R}^+$.

Moreover, by simple calculations, the c.d.f. of the folded Normal random variable $|Z_i|$ is $F_{|Z_i|}(z) = 2\Phi(z) - 1$.

First of all, the following approximations hold for Λ large (Bouchaud et al. (2000))

$$\begin{aligned} \mathbb{P}\left(\max_{i=1, \dots, n} |Z_i| \leq \Lambda\right) &= [F_{|Z_i|}(\Lambda)]^n \\ &= [2\Phi(\Lambda) - 1]^n \\ &= [1 - 2(1 - \Phi(\Lambda))]^n \\ &\approx 1 - 2n(1 - \Phi(\Lambda)) \end{aligned} \tag{34}$$

where the first equality is consequence of the order statistic theory and, in particular, of the c.d.f. of the maximum of n identical distributed random variables.

Analogously,

$$\begin{aligned} \mathbb{P}\left(\max_{i=1, \dots, n} Z_i \leq \Lambda\right) &= [F_Z(\Lambda)]^n \\ &= [\Phi(\Lambda)]^n \\ &= [1 - (1 - \Phi(\Lambda))]^n \\ &\approx 1 - n(1 - \Phi(\Lambda)) \end{aligned} \tag{35}$$

Therefore, applying the approximations in Eq. 34 and 35,

$$\begin{aligned} \mathbb{P}\left(\max_{i=1, \dots, n} |Z_i| > \Lambda\right) &= 1 - \mathbb{P}\left(\max_{i=1, \dots, n} |Z_i| \leq \Lambda\right) \\ &\approx n2(1 - \Phi(\Lambda)) \\ &= 2[n(1 - \Phi(\Lambda))] \\ &\approx 2\mathbb{P}\left(\max_{i=1, \dots, n} Z_i > \Lambda\right) \end{aligned} \tag{36}$$

where the last approximation holds since $\mathbb{P}\left(\max_{i=1, \dots, n} Z_i > \Lambda\right) = 1 - \mathbb{P}\left(\max_{i=1, \dots, n} Z_i \leq \Lambda\right) \approx n(1 - \Phi(\Lambda))$.

B Numerical and Empirical Tests

B.1 Jump Size Distribution Filtering and Isolation

Starting from the characteristic function estimate of the convolution of two random variables and knowing the distribution function of the first random variable analytically, the probability density function of the second one can be estimated via Fourier Transform technique.

B.1.1 Characteristic Functions and Convolution Property

Let X_1 and X_2 be two random variables with real-valued p.d.f.s $f_{X_1}(x)$ and $f_{X_2}(x)$, respectively. Moreover, let $\Psi_{X_1}(u)$ and $\Psi_{X_2}(u)$ be the corresponding characteristic functions and let $Y := X_1 + X_2$ be the random variable resulting from the convolution of X_1 and X_2 .

The characteristic function of Y equals

$$\Psi_Y(u) = \Psi_{X_1}(u) \cdot \Psi_{X_2}(u) \tag{37}$$

B.1.2 From Fourier Transforms to p.d.f.s

Let Z be a random variable with real-valued p.d.f. $f_Z(z)$ and let $\Psi_Z(u)$ be the corresponding characteristic function.

Recalling that the characteristic function of a generic real-valued random variable corresponds to the Fourier Transform of the underlying p.d.f., i.e. $\Psi_Z(u) := \mathbb{E}[e^{iuZ}] = \int_{\mathbb{R}} e^{iuz} f_Z(z) dz = \hat{f}_Z(u)$, the following property

$$f_Z(z) = \frac{1}{\pi} \operatorname{Re} \left(\int_0^\infty \hat{f}_Z(u) e^{iuz} du \right) \quad (38)$$

allows to identify the p.d.f of Z starting from its characteristic function.

B.1.3 Jump Size Distribution Isolation

Assuming to know the characteristic function $\Psi_Y(u)$ of the convolution of the Gaussian random variable X_1 corresponding to the Brownian motion part and the jump size random variable X_2 , the characteristic function of X_2 can be computed inverting Eq. 37, i.e.

$$\Psi_{X_2}(u) = \frac{\Psi_Y(u)}{\Psi_{X_1}(u)} \quad (39)$$

with $\Psi_{X_1}(u) = e^{iu\mu - \frac{1}{2}\sigma^2 u^2}$ and μ and σ^2 the mean and variance of the Gaussian random variable, respectively.

Finally, the p.d.f. of the jump size random variable can be estimated by numerically evaluating formula 38, where the Fourier Transform of $f_{X_2}(x)$ coincides with the characteristic function $\Psi_{X_2}(u)$.

Note that, in practice, the characteristic function $\Psi_Y(u)$ can be empirically estimated by using the realizations of the variable Y .

B.1.4 Filtering Technique

By means of the OS or threshold estimator the realizations classified as sum of the Brownian component and the jump component are identified and thus their empirical characteristic functions can be estimated. Nevertheless, since the central part of the convoluted distributions is missed by definition of the threshold estimator and by implementation choices of the OS estimator, a filter technique to complete such distributions must be applied.

In practice, we interpolated the last central points of the histogram of the cumulative jump size with a cubic function and we added to the sample $y_1 := f(x_1), \dots, y_n := f(x_n)$ realizations with sizes x_1, \dots, x_n , respectively. f is the interpolating function used.

As an example, Figure 18a and Figure 18b show the filtering procedure applied to the distributions reported in Figure 7 of Subsection 4.1.

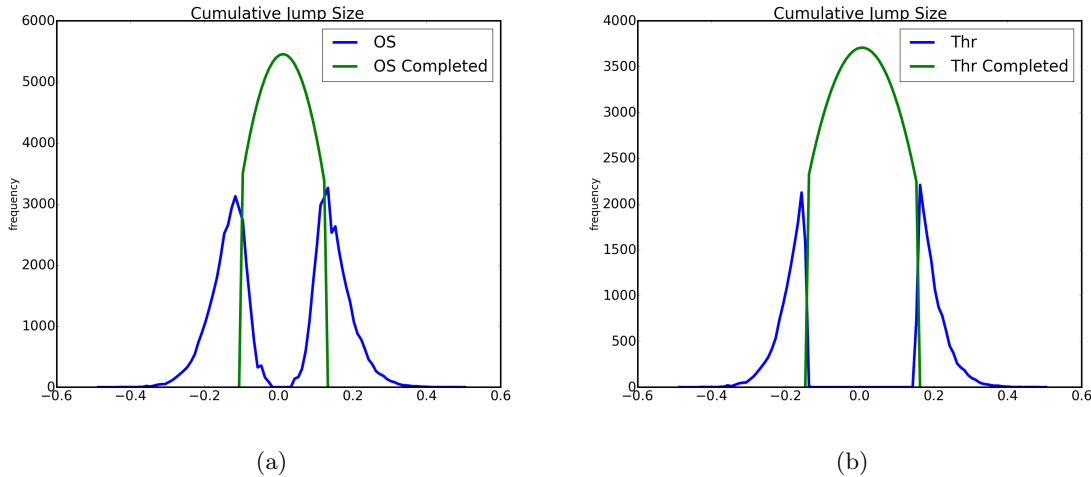


Figure 18: Cumulative jump size (i.e. including both the Brownian Motion and the pure jump realizations) histograms filtering with a cubic interpolating function. In the left panel, the cumulative jump size histogram created using the jump realizations identified by the OS estimator (blue line) and its central part filling (green line) are shown, while, in the right panel, the same data obtained using the threshold estimator are reported. Model parameters: $b = 0$, $\sigma = 0.5$, $\lambda = 10$, $\delta = 1.5$ and $\mu = 0$. Simulation parameters: number of time-steps for each simulation $N_{TS} = 5000$, simulation time horizon $T = 20$, number of simulations $M = 1000$. Estimator parameters: OS estimator tolerance level $p = 5\%$, bandwidth $h = N_{TS}$.

References

- Yacine Ait-Sahalia. Disentangling diffusion from jumps. *Journal of Financial Economics* **74**(3), 487–528.
- T. W. Anderson and D. A. Darling. A Test of Goodness of Fit. *Journal of the American Statistical Association* **49**(268), 765–769. ISSN: 01621459. URL: <http://www.jstor.org/stable/2281537>.
- Basel Committee on Banking Supervision. Fundamental review of the trading book, consultative document. URL: www.bis.org/publ/bcbs219.htm.
- Basel Committee on Banking Supervision. Fundamental review of the trading book: A revised market risk framework, consultative document. URL: www.bis.org/publ/bcbs265.htm.
- Basel Committee on Banking Supervision. Fundamental review of the trading book: Outstanding issues, consultative document. URL: www.bis.org/bcbs/publ/d305.htm.
- Ole E. Barndorff-Nielsen, Neil Shephard and Matthias Winkel. Limit theorems for multipower variation in the presence of jumps. *Stochastic Processes and their Applications* **116**(5), 796–806.
- J.P. Bouchaud and M. Potters. *Theory of Financial Risks: From Statistical Physics to Risk Management*. Aléa Saclay collection. Cambridge University Press, 2000. ISBN: 9780521782326. URL: <https://books.google.it/books?id=W3ANngEACAAJ>.
- Peter Carr and Helyette Geman. The Fine Structure of Asset Returns: An Empirical Investigation. *The Journal of Business* **75**(2), 305–332.
- Fen-Ying Chen. VaR: Exchange Rate Risk and Jump Risk. *Journal of Probability and Statistics* **2010**(Article ID 196461).
- H. A. David and H. N. Nagaraja. *Order statistics*. 3rd ed. Wiley Series in Probability and Statistics. John Wiley, 2003. ISBN: 9780471389262,0-471-38926-9. URL: <http://gen.lib.rus.ec/book/index.php?md5=276A8FB1A79A3E37D97A1E47E4BEDED4>.

- José Figueroa-López and Cecilia Mancini. *Optimum thresholding using mean and conditional mean square error*. Working Papers - Mathematical Economics 2017-01. Università degli Studi di Firenze, Dipartimento di Scienze per l'Economia e l'Impresa, 2017. URL: <http://EconPapers.repec.org/RePEc:fllo:wpaper:2017-01>.
- Helyette Geman. Pure jump Levy processes for asset price modelling. *Journal of Banking & Finance* **26**(7), 1297–1316.
- Michael S. Gibson. *Incorporating event risk into value-at-risk*. Finance and Economics Discussion Series 2001-17. Board of Governors of the Federal Reserve System (U.S.), 2001.
- Lim Kian Guan, Liu Xiaoqing, and Tsui Kai Chong. Asymptotic dynamics and value-at-risk of large diversified portfolios in a jump-diffusion market. *Quantitative Finance* **4**(2), 129–139.
- Cecilia Mancini. Non-parametric Threshold Estimation for Models with Stochastic Diffusion Coefficient and Jumps. *Scandinavian Journal of Statistics* **36**(2), 270–296.
- Cecilia Mancini. *Speed of convergence of the threshold estimator of integrated variance*. Working Papers - Mathematical Economics 2010-03. Università degli Studi di Firenze, Dipartimento di Scienze per l'Economia e l'Impresa, 2010. URL: <http://EconPapers.repec.org/RePEc:fllo:wpaper:2010-03>.
- Cecilia Mancini and Roberto Renò. Threshold estimation of Markov models with jumps and interest rate modeling. *Journal of Econometrics* **160**(1), 77–92. URL: <http://EconPapers.repec.org/RePEc:eee:econom:v:160:y:2011:i:1:p:77-92>.
- Jun Pan and Darrell Duffie. Analytical value-at-risk with jumps and credit risk. *Finance and Stochastics* **5**(2), 155–180.
- K. Sato. *Lévy Processes and Infinitely Divisible Distributions*. Cambridge Studies in Advanced Mathematics. Cambridge University Press, 1999. ISBN: 9780521553025. URL: <https://books.google.it/books?id=tbZPLquJjSoC>.
- Neil Shephard and Ole E. Barndorff-Nielsen. *Power and bipower variation with stochastic volatility and jumps*. Economics Series Working Papers 2003-W18. University of Oxford, Department of Economics, 2003.
- L. Spadafora and G.P. Berman. *Theoretical Foundations for Quantitative Finance*. World Scientific Publishing Company Pte Limited, 2017. ISBN: 9789813202474. URL: <https://books.google.it/books?id=YBMNMQAACAAJ>.
- L. Spadafora M. Dubrovich M. Terraneo. Value-at-Risk time scaling for long-term risk estimation. URL: <https://arxiv.org/abs/1408.2462>.
- Pawel J. Szerszen. *Bayesian analysis of stochastic volatility models with Lévy jumps: application to risk analysis*. Finance and Economics Discussion Series, 2009-40. Board of Governors of the Federal Reserve System (U.S.), 2009.
- P. Tankov and R. Cont. *Financial Modelling with Jump Processes, Second Edition*. Chapman and Hall/CRC Financial Mathematics Series. Taylor & Francis, 2015. ISBN: 9781420082197. URL: <https://books.google.it/books?id=-fZtKgAACAAJ>.